



People's Democratic Republic of Algeria
Ministry of Higher Education
and Scientific Research



FERHAT ABBAS UNIVERSITY - SETIF 1

FACULTY OF SCIENCE

DEPARTMENT: PHYSICS

MASTER'S THESIS

FIELD: Material Sciences

AREA: Physics

SPECIALITY: Materials Physics

Theme

Study of the structural and optical properties of co-doped Tin Sulfide nanoparticles

Presented by:

Khatir Ismahane

Examination jury:

Dr.SAOUDI AMER.....Chairman

Dr.MESSALTI SAID ABDELGHAFOURSupervisor

Dr.REFFAS MOUNIRExaminer

Promotion: June/2025

ACKNOWLEDGMENTS

This work was carried out at the Laboratory of Chemistry, Molecular Engineering, and Nanostructures and emerging materials research unit from Ferhat Abbas University –Sétif -1.

First and foremost, I would like to thank Almighty **God**, the merciful, for granting me health, strength, and patience to complete this thesis.

I like to thank **Dr. MESSALTI ABD EL GHAFOR SAID**, for supervising this work

He introduced me to the research field and guided me in every detail, showing me that effort, patience, and dedication are required to be a good researcher. Most importantly, he taught me the importance of having a scientific conscience. Permit me to sincerely thank him for his support, confidence, and availability, all of which allowed me to achieve this work successfully.

I extend my sincerest thanks to **Pr. HADDADI KHALIFA**, and **Dr. HAMICI MALIA** for their valuable guidance, their help and their wise advice during the completion of this work.

My greetings also go to all the directors, technicians, or laboratory engineers who facilitated my access to perform the characterizations, for their welcome.

Dedication

To my dearest **Parents**,

Your unwavering love, countless sacrifices, and endless encouragement have been the bedrock of my life. You instilled in me the values of perseverance and dedication, and your belief in my abilities has always been my greatest motivation. This achievement is as much yours as it is mine. Thank you for everything.

To my dear **Husband**,

Your steadfast support, understanding, and patience have been invaluable throughout this journey. You provided a sanctuary of calm and strength, always believing in me even when I doubted myself. Your encouragement made every challenge surmountable, and I am eternally grateful for your presence in my life. Not forgetting my **precious children** who will find their mother's memory in the coming years and may they be proud of it, inshallah.

To my dear **Brothers** and **Sister**,

Your constant cheer, moral encouragement, and the unwavering belief you've shown in me have truly made a difference. Knowing I had your support, your kind words, and your understanding made this demanding period so much lighter. Thank you for being my incredible siblings and for always standing by me.

This memoir is a testament to the strength and love I draw from each of you. Your collective moral aid has been the light guiding me through this academic endeavor. I dedicate this work to my wonderful family, with all my love and deepest appreciation.

List of figures.

| | |
|--|-------------------------------------|
| FIGURE 1 : TEM IMAGES OF DIFFERENT FORM OF NPs SYNTHESIZED BY DIFFERENT TECHNIQUES..... | 9 |
| FIGURE 2 : ORGANIC NANOPARTICLES (7) | 10 |
| FIGURE 3 : TOP-DOWN AND BOTTOM UP APPROACH(9)..... | 12 |
| FIGURE 4 :DIAGRAM REPRESENTING THE BAND THEORY OF METALS, SEMICONDUCTORS, AND INSULATORS..... | 15 |
| FIGURE 5 : DIRECT BAND GAP AND INDIRECT BAND GAP SEMMICONDUCTOR | 16 |
| FIGURE 6 : DIFFERENT TYPES OF SEMICONDUCTOR NANOPARTICLES(10) | 18 |
| FIGURE 7 : DIAGRAM SHOWING ENERGY BAND STRUCTURESIN ATOM ,BULK MATERIAL AND QUANTUM NANOSTRUCTURE(13) | 19 |
| FIGURE 8 : STRUCTURAL MODEL OF ORTHORHOMBIC TIN SULFIDE SnS(17) | 21 |
| FIGURE 9 : ELEMENTARY CELL OF THE ZINC BLEND STRUCTURE | 21 |
| FIGURE 10 : ABSORPTION SPECTRA FOR THE TIN SULFIDE SnS NANOPARTICLES(16)..... | 22 |
| FIGURE 11 : THE CALCULATED ELECTRONIC ENERGY BAND STRUCTURE OF SnS(20) | 24 |
| FIGURE 12STAINLESS STEEL AUTOCLAVE(27)..... | 28 |
| FIGURE 13 : SYNTHESIS PROTOCOL | 29 |
| FIGURE 14 : PHASE OF PURE SnS NANOPARTICLE SYNTHESIS | 30 |
| FIGURE 15 : PHASE OF PURE SnS NANOPARTICLE SYNTHESIS | 31 |
| FIGURE 16 : COMPONENTS OF DOPING..... | 32 |
| FIGURE 17 : HANGING AND WASHING | 33 |
| FIGURE 18 : PURE AND DOPED SnS POWDERS AFTER DRYING | 34 |
| FIGURE 19 : COMPARISON OF THE SPECTRUM OF NON-DOPED SnS NPs WITH THE ICOD..... | 35 |
| FIGURE 20 : TIN SULFIDE STRUCTURE DRAWN BY VESTA WIN 64 | 35 |
| FIGURE 21 : XRD OF PURE SnS | 36 |
| FIGURE 22 : COMPARISON OF THE SPECTRUM OF NON-DOPED AND Fe-DOPEDSnS NPs | 37 |
| FIGURE 23 : COMPARISON OF THE SPECTRUM OF NON DOPED AND Cu- DOPED SnS NPs..... | 38 |
| FIGURE 24 : COMPARISON OF THE SPECTRUM OF NON-DOPED AND CO-DOPED SnS | 39 |
| FIGURE 25 : FTIR SPECTRA OF THE UNDOPED AND Fe,Cu AND Fe AND Cu SnS NPs | 40 |
| FIGURE 26 : TGA AND DTA ANALYSIS..... | 42 |
| FIGURE 27 : GENERAL PROCESS OF PHOTOCATALYSIS | 47 |
| FIGURE 28 : CHARACTRISTIC PF BM AND ITS MOLECULAR STRUCTURE | 48 |
| FIGURE 29: PROTOCOL OF THE STUDY IN THE DARK..... | 49 |
| FIGURE 30 : EVOLUTION OF THE ABSORBANCE SPECTRUM OF METHYLENE BLUE..... | 50 |
| FIGURE 34:PHOTOCATALYSIS EXPERIMENT | ERROR! BOOKMARK NOT DEFINED. |
| FIGURE 35:DEGRADATION OF BM | 54 |
| FIGURE 36:EVOLUTION OF THE CONCENTRATION OF MB | ERROR! BOOKMARK NOT DEFINED. |
| FIGURE 37:PRINCLE OF PHOTOLUMINESCENCE | ERROR! BOOKMARK NOT DEFINED. |
| FIGURE 38:EXCITEMENT SPECTRUM OF SnS AND DOPED SnS NPs..... | 58 |
| FIGURE 39:NORMALIZED EXCITEMENT SPECTRA OF SnS NPs:1%Fe..... | ERROR! BOOKMARK NOT DEFINED. |
| FIGURE 40NORMALIZED EXCITEMENT SPECTRUM OF SnS AND Cu DOPED SnS NPs .. | ERROR! BOOKMARK NOT DEFINED. |
| FIGURE 41:NORMALIZED EXCITEMENT SPECTRUM OF SnS AND CO-DOPED SnS NPS .. | ERROR! BOOKMARK NOT DEFINED. |
| FIGURE 42EMISSION SPECTRUM OF SnS AND Fe Cu DOPED SnS NPs | 60 |
| FIGURE 43:EMISSION SPECTRUM OF SnS AND Fe DOPED SnS NPs | ERROR! BOOKMARK NOT DEFINED. |
| FIGURE 44:EMISSION SPECTRUM OF SnS AND Fe DOPED SnS NPs | ERROR! BOOKMARK NOT DEFINED. |

List of tables.

| | |
|---|----|
| TABLE 1:POSITION OF THE ELEMENTS Sn AND S IN THE PERIODIC TABLE | 20 |
| TABLE 2:MASS OF IRON CHLORIDE AS A FUNCTION OF THE PERCENTAGE OF DOPANT | 31 |
| TABLE 3 : MASS OF IRON CHLORIDE AS A FUNCTION OF THE PERCENTAGE OF DOPANT | 32 |
| TABLE 4:MASS OF IRON CHLORIDE AS A FUNCTION OF THE PERCENTAGE OF DOPANT..... | 32 |
| TABLE 5:GRAIN SIZE AND LATTICE PARAMETER OF UNDOPED AND DOPED SnS NPs | 39 |

Contents

| | |
|--|----|
| Contents..... | 5 |
| Chapter I : State of the art | 8 |
| 1. Nanoscience and nanotechnology | 8 |
| 2. Nanoparticles..... | 8 |
| 3. Classification of nanoparticles | 10 |
| 3.1. Organic nanoparticles | 10 |
| 3.2. Inorganic nanoparticles..... | 10 |
| 4. Different synthesis methods. | 11 |
| 4.1. Top down approach..... | 11 |
| 4.2. Bottom- up approach..... | 11 |
| 4.3. Physical methods of nanoparticles synthesis | 12 |
| 4.4. Chemical methods of nanoparticles synthesis..... | 12 |
| 4.5. Mechanical methods of nanoparticles synthesis | 13 |
| 5. Properties of nanoparticles | 13 |
| 6. Applications..... | 13 |
| 7. SEMICONDUCTORS NANOPARTICLES..... | 14 |
| 7.1. definition of semiconductors..... | 15 |
| 7.2. Band gap of semiconductor..... | 15 |
| 7.3. Classification of semiconductors. | 16 |
| 7.4. Binary nanoparticles | 17 |
| 7.5. Chalcogenides nanoparticles..... | 17 |
| 7.6. The semiconductor quantum dots | 18 |
| 8. Tin sulfide..... | 19 |
| 8.1. General information on tin sulfide | 19 |
| 8.2. The compound Tin (II) sulfide SnS | 20 |
| 8.3. properties of tin sulfide | 20 |
| 8.4. Optical properties..... | 22 |
| 8.5. Electrical properties | 23 |
| 8.6. Application of Tin sulfide | 24 |
| Conclusion..... | 25 |
| Chapter II synthesis and characterization..... | 27 |
| 1. SYNTHESIS | 27 |
| 1.1. INTRODUCTION | 27 |
| 1.2. Hydrothermal synthesis..... | 27 |
| 1.2.1. PRICIPLE..... | 27 |
| 1.2.2. EQUIPMENT..... | 28 |
| 1.2.3. EXPERIMENTAL PROTOCOL | 28 |

| | | |
|--------|--|----|
| 1.3. | Synthesis of tin Sulfide nanoparticles | 29 |
| 1.3.1. | Pure SnS | 30 |
| 1.3.2. | Doped SnS..... | 31 |
| 1.3.3. | Washing Procedure | 33 |
| 2. | Characterization..... | 34 |
| 2.1. | X-ray Diffraction (XRD) | 34 |
| 2.1.1. | Doping effect..... | 37 |
| 2.2. | Fourier Transform Infrared Spectroscopy (FTIR) | 40 |
| 2.3. | Thermal analysis | 41 |
| | Conclusion..... | 44 |
| | Chapter III : application | 45 |
| 1. | Photocatalysis..... | 45 |
| 1.1. | Introduction..... | 45 |
| 1.2. | Definition of photocatalysis and processus..... | 46 |
| 1.2.1. | Definition | 46 |
| 1.2.2. | Types of photocatalysis..... | 46 |
| 1.2.3. | principle of the heterogeneous photocatalysis..... | 46 |
| 1.3. | Study of (MB) adsorption in the dark | 47 |
| 1.3.1. | Preparation of methylene blue solution..... | 48 |
| 1.3.2. | Operating conditions and progress of the experiment..... | 50 |
| 1.4. | Photocatalytic tests..... | 52 |
| 2. | Photoluminescence | 56 |
| 2.1. | Introduction..... | 56 |
| 2.2. | Property of each dopant | 57 |
| 2.2.1. | The Fe ²⁺ Ion | 57 |
| 2.2.2. | The Cu ²⁺ Ion..... | 57 |
| 2.3. | Excitation spectrum | 58 |
| 2.3.1. | SnS doped Fe Cu NPs | 58 |
| 2.4. | Emission spectrum | 60 |
| 2.4.1. | SnS doped Fe Cu NPs | 60 |
| | Conclusion..... | 62 |
| | General conclusion | 62 |
| | Bibliographic references..... | 64 |

General introduction

Over the past 20 years, research on the development of new structured materials with nanometric dimensions has surged. These materials are on the atomic scale and have a unique set of features. Despite their tiny size, they possess the distinct mechanical, optical, electrical, and optical properties of molecules as well as a crystalline structure like that of bulk materials. Among these nanostructured materials, semiconductors have grown in significance for both fundamental and applied research. Their reputation is mostly due to their superior properties over other materials of similar size. Particularly, inorganic semiconductors are favored over their organic counterparts for several reasons. Tin chalcogenide nanostructures, especially tin mono-sulfide (SnS), have drawn a lot of interest in the field of photovoltaics because of their semiconducting nature and staggered band gap structure.

This work's primary objective is to produce tin sulfide (SnS) nanoparticles doped with Iron (Fe^{2+}) and copper (Cu^{2+}) using the hydrothermal method. This method was chosen because to its ability to produce extremely pure, well-defined nanostructures. Examining how various parameters impact the properties of the generated nanoparticles is the aim of the study. To achieve these objectives, a variety of experimental techniques will be employed. X-ray diffraction (XRD) will be used to determine the crystalline structure and phase purity of the generated materials. Fourier-transform infrared spectroscopy (FTIR) will be used to comprehend the molecular structure and chemical bonding. Thermogravimetric Analysis (TGA) will be used to comprehend the thermal stability, composition, and decomposition pathways.

An intriguing chance to further improve these properties is provided by the doping of transition metals. By adding these metals to the zinc sulfide nanoparticle composition, intermediate energy levels are produced inside the material's energy gap. These extra energy levels allow for better control and modification of the nanoparticles' luminous characteristics, potentially resulting in more potent, consistent, and effective light emissions.

The optical characteristics of the doped SnS nanoparticles, namely their emission characteristics, will be investigated using photoluminescence spectroscopy. This research attempts to contribute to a wider understanding of nanostructured semiconductors and their possible applications in numerous technical domains by methodically examining these parameters and their effects.

Methylene blue pollutant (MB) degradation under visible light was used to examine the resulting particles' photocatalytic activity.

Chapter I : State of the art

1. Nanoscience and nanotechnology

We should distinguish between nanoscience, and nanotechnology. Nanoscience is the study of structures and molecules on the scales of nanometers ranging between 1 and 100 nm, and the technology that utilizes it in practical applications such as devices etc. is called nanotechnology. (1)

One of the 21st century's most promising technologies is nanotechnology. It is the capacity to observe, measure, manipulate, assemble, control, and manufacture materials at the nanoscale scale in order to translate the theory of nanoscience into practical applications. (2)

Nanoscience is not about fundamentally new physics, but rather new combinations of phenomena manifesting at the nanoscale. While it may seem superfluous in the context of conceptual nanotechnology, it could be a valid synonym for mesoscale approximation, as it encompasses the fields of biology, chemistry, and physics.(3)

The development and use of chemical, physical, and biological systems at scales spanning from 1 to 100 nm, from single molecules or atoms to submicron dimensions, is referred to as nanotechnology. One atom or molecule at a time, stable structures are created by integrating nanomaterials into bigger systems.(4)

2. Nanoparticles.

nanoparticle, ultrafine unit with dimensions measured in nanometres (nm; 1 nm = 10^{-9} metre). Nanoparticles exist in the natural world such as volcanic ash and are also created as a result of human activities. Because of their submicroscopic size, they have unique material characteristics, and manufactured nanoparticles may find practical applications in a variety of areas. They can be powder, suspension, solution, or gel.(5)

Many synthesis and deposition techniques have been developed, which has led to a broad variety of research and development on nanomaterials worldwide. Nanospheres, nanorods, nanochains, decahedral nanoparticles, nanostars, nanoflowers, nanoreefs, nanowhiskers, nanofibers, and nanoboxes are just a few of the various configurations that nanoparticles can take.

Definition of nanoparticles.

“Nanoparticle” has been defined in different ways in the literature. According to ASTM 2456-06 Standard Terminology Relating to Nanotechnology it is defined as “a particle with lengths in two or three dimensions greater than 1nm and smaller than 100 nm and which may or may not exhibit a size-related intensive property”.(6)

In order to differentiate them from one- and two-dimensional nanomaterials, which have one or two dimensions bigger than the nanoscale, respectively, NPs are also referred to as zero-dimensional nanomaterials. Their size, chemical reactivity, movement, energy absorption, and other characteristics set them apart from their bulk counterparts.

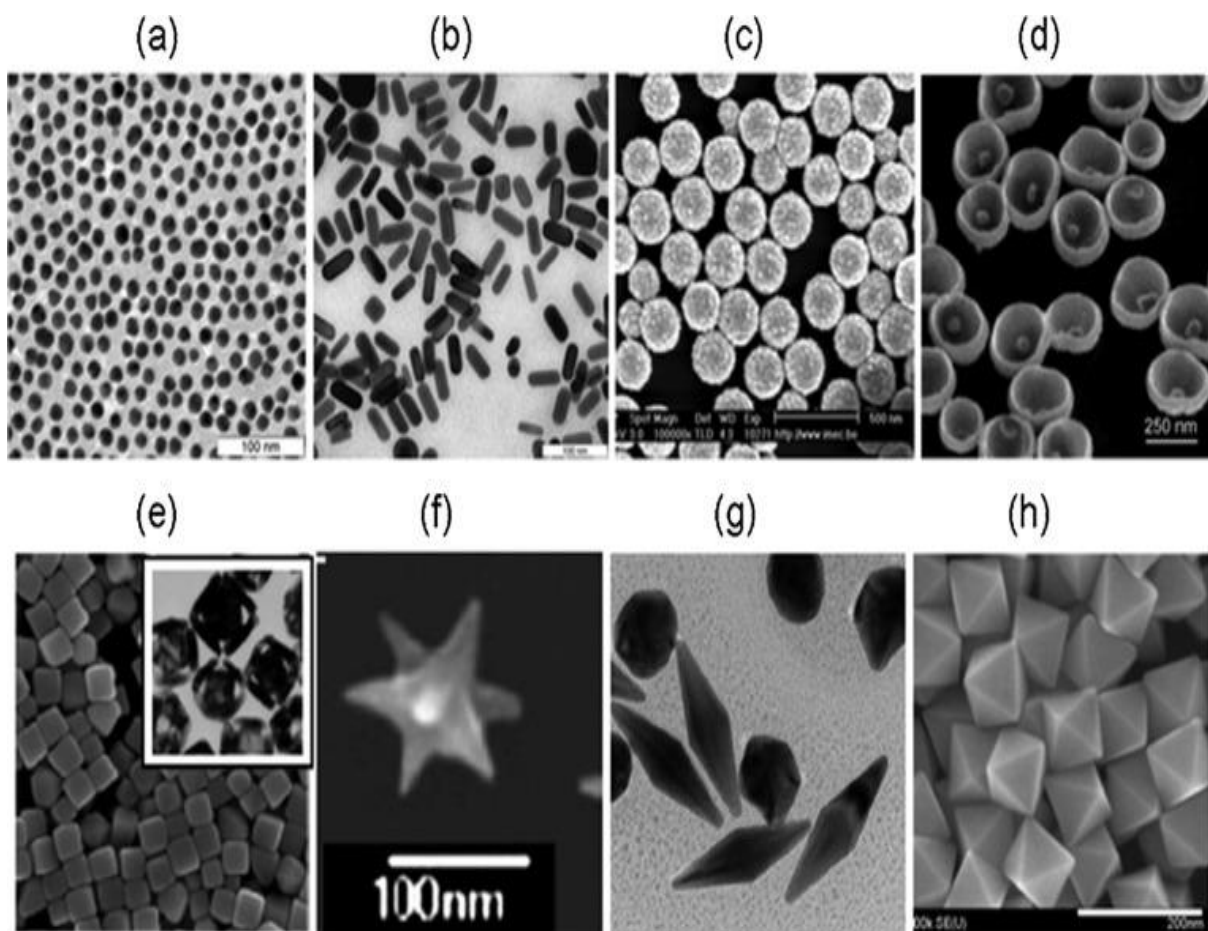


Figure 1 : TEM images of different form of NPs synthesized by different techniques.

3. Classification of nanoparticles

Nanoparticles are generally classified as organic, inorganic.

3.1. Organic nanoparticles

Ferritin, liposomes, dendrimers, and micelles are examples of organic nanoparticles that are sensitive to heat and electromagnetic radiation, biodegradable, and non-toxic.

Because of these special qualities, they are perfect for medication delivery; their carrying capacity, stability, and distribution methods all affect how effective they are.

Since organic nanoparticles may be injected into particular bodily locations, they are a popular and efficient option for targeted medication administration in the biomedical area. (7)

Carbon-based nanoparticles are those that are entirely composed of carbon.

They are displayed in nanoscale and can be categorized as fullerenes, graphene, carbon nanotubes (CNT), carbon nanofibers, carbon black, and occasionally activated carbon. (7)

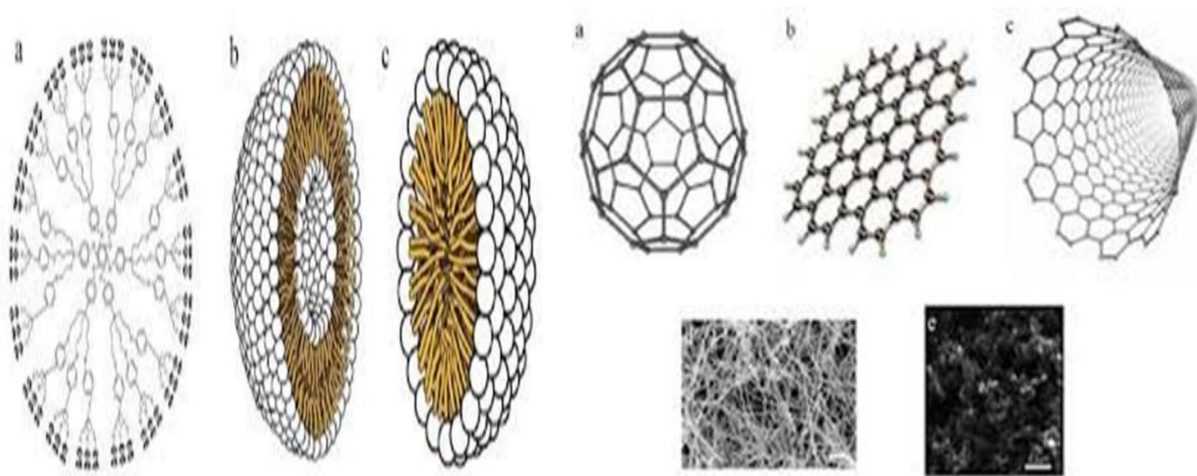


Figure 2 : organic nanoparticles (7)

3.2 Inorganic nanoparticles

They are particles that are not made up of carbon or organic materials. The typical examples for this class are metal, metal oxide and ceramic NPs

❖ **Metal based:** Destructive or constructive processes are used to create metal-based nanoparticles. Aluminum, cadmium, cobalt, copper, gold, iron, lead, silver, and zinc are among the frequently utilized metals. Size, surface features, crystalline and amorphous structures, forms, colors, and

reactivity to environmental elements including heat, moisture, sunshine, and air are some of these nanoparticles' distinctive qualities. A variety of metals can be used to create these nanoparticle(7)

- ❖ **Metal oxides based:** In order to alter their characteristics, metal oxide-based nanoparticles are created. For example, oxidizing iron nanoparticles to iron oxide in the presence of oxygen can increase reactivity and efficiency.(7)
- ❖ **Ceramic NPs:** Ceramic nanoparticles (NPs) are inorganic solids composed of carbonates, carbides, and phosphates, including calcium and titanium. They are often created by heating and then cooling, and they can be amorphous, polycrystalline, dense, porous, or hollow.

4. Different synthesis methods.

Nanoparticles synthesis is an essential part of nanotechnology and nanoscience. During synthesis of nanoparticles, several controlling factors are involved in the nucleation and subsequent production of stabilized nanoparticles. These factors include temperature, reactant concentrations, reaction time.(8)

The two main approaches for creating nanoparticles are the top down and the bottom- up approaches.

4.1. Top-down approach.

Top-down is a fabrication process that starts with a bulk block material identical to the base substrate and reduces it using physical methods like crushing, milling, or grinding. This method is easier and relies on the removal of bulk materials or downsizing of bulk manufacturing techniques. It improves the synthesis technique for producing micron-sized particles, but faces surface structural faults. Top-down is used in industry to fabricate various man-made materials.(8)

4.2. Bottom- up approach.

Bottom-up approaches involve material component miniaturization and self-assembly to create nanostructures. This method is popular for synthesizing nanosized materials due to their unique properties. It is more economical and produces less waste. This method is used in continuous synthesis of inorganic nanoparticles, such as zinc oxide, magnetite, and brushite. It is also used for the preparation of luminescent nanoparticles. Bottom-up nanofabrication pushes the limits of miniaturization, provides limitless opportunities for fabrication and design, and is cost-effective compared to top-down nanofabrication.(8)

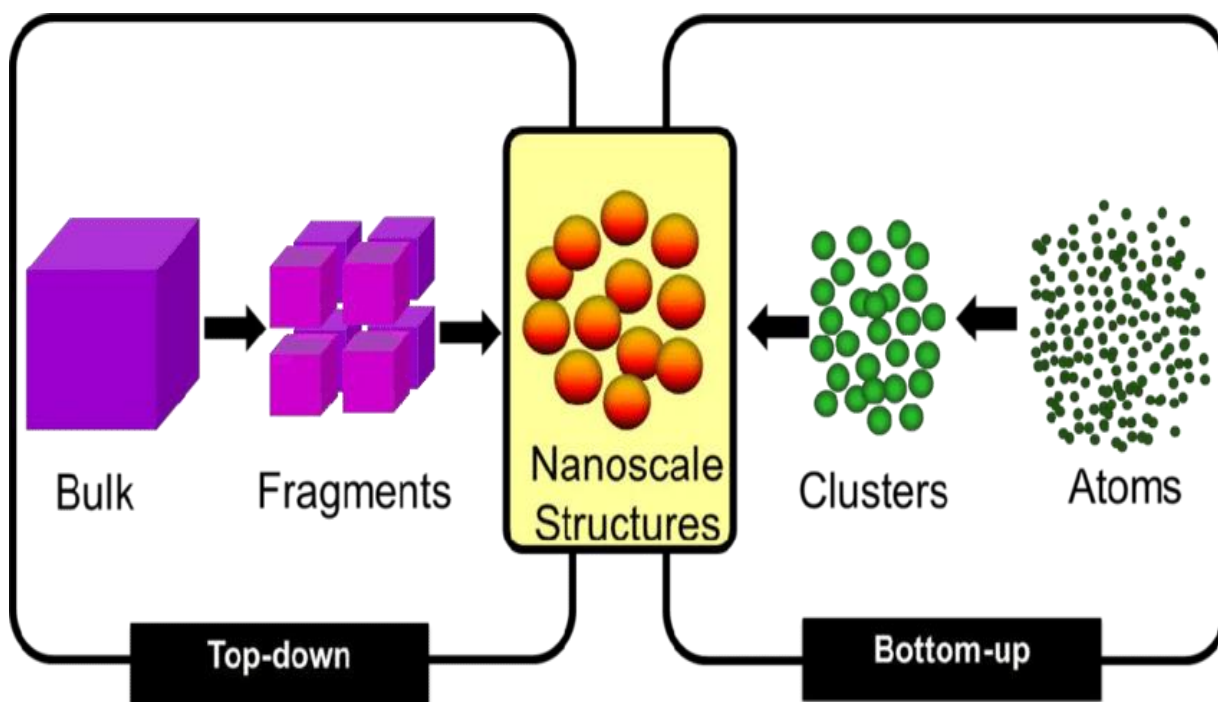


Figure 3 : TOP-Down and Bottom up approach(9)

Synthetic processes can be grouped according to various mechanisms that lead to their formation: chemical processes, physical processes, and mechanical processes.

4.3. Physical methods of nanoparticles synthesis

Nanoparticles are synthesized using physical methods like thermal energy, radiation, and mechanical pressure. These methods are better for thin films and homogeneity of nanoparticles, leading to better formation of Li dendrite without solvent contamination. Top-down processes like poly-pulse laser ablation, laser pyrolysis, physical vapor deposition, high-energy ball milling, and inert gas condensation yield mono-disperse nanoparticles.(8)

4.4. Chemical methods of nanoparticles synthesis

Metallic colloidal particles are created via the chemical production of nanoparticles using both organic and inorganic reducing agents. Salvo thermal synthesis, hydrothermal synthesis, polyol synthesis, micro emulsion technique, Sol–gel method, plasma and chemical vapor synthesis, and microwave aided synthesis are some of the techniques.(8)

4.5. Mechanical methods of nanoparticles synthesis

Key mechanical procedures include the mechanical activation of powder metallurgy and mechanosynthesis. Densification and consolidation. the severe distortion brought on by friction, rolling, or torsion.

In this work, we will use an hydrothermal method, which is a bottom-up approach. chemical methods are widely used because they are effective at providing better control over the size and shape of the final nanoparticles.

5. Properties of nanoparticles

Nanoparticles have properties that are modified by their size, leading to an increase in the surface-to-volume ratio. This changes the properties of nanoparticles, focusing more on surface reactions and changes. The higher the surface-to-volume ratio, the more specific phenomena can be observed. Nanoparticles have a significant difference between volume and surface area, with smaller sizes resulting in more molecules on the surface. This leads to increased reaction capacity, free radical generation, adsorption, aggregation, and dissolution. This results in lively surfaces and small objects with high penetration capacity.

6. Applications

Nanoparticles have a wide range of applications across various fields due to their unique properties.

Biomedical applications

- **Drug delivery:** nanoparticles can be used to deliver drugs to specific targets in the body, improving efficacy and reducing side effects.
- **Imaging:** nanoparticles can be used as contrast agents for medical imaging techniques like MRI and CT scans.
- **Therapy:** nanoparticles can be used for photothermal therapy, gene therapy, and other therapeutic applications.

Environmental applications

- **Remediation:** nanoparticles can be used to remove pollutants from water and soil.
- **Sensing:** nanoparticles can be used to detect pollutants and other environmental contaminants.

Industrial applications

- **Catalysis:** nanoparticles can be used as catalysts to improve the efficiency of chemical reactions.
- **Coating:** nanoparticles can be used to create protective coatings for various materials.
- **Electronics:** nanoparticles are used in electronics devices such as semiconductors and solar cells.

Consumer products

- **Cosmetics:** Nanoparticles are used in some cosmetics for UV protection and other benefits.
- **Food:** Nanoparticles are used in some food products for various purposes such as enhancing flavor and preservation

Other applications

- **Energy:** Nanoparticles are used in energy storage and conversion technologies
- **Agriculture:** Nanoparticles can be used in agriculture for crop protection and nutrient delivery

7. SEMICONDUCTORS NANOPARTICLES.

In addition to the scale of their characteristic dimensions, nanomaterials differ from micro-sized and bulk materials in that they may have novel physical characteristics and provide new opportunities for numerous technological uses. The recent development of several important technologies has been greatly aided by semiconductor nanoparticles. Due to their unique size-dependent material characteristics and abundance of quantum events, semiconductor nanoparticles' optical responses have been the subject of intense experimental and theoretical research over the past 20 years. The materials for next-generation flat panel displays, photovoltaic, optoelectronic, laser, sensor, and photonic band gap devices are thought to be semiconductors with a broadly adjustable energy band gap. When compared to the bulk material, artificially created semiconductor structures with smaller dimensions provide a wide range of intriguing new features that open up new avenues for semiconductor engineering. A spatial confinement of carriers may be created by simply combining two semiconductor materials with differing band gap energies.

7.1. definition of semiconductors.

Semiconductors are solid materials with a crystalline structure and extremely few free electrons at ambient temperature that are neither excellent conductors (like metals) nor insulators (like glass). Between the conductors and insulators are energy gaps and resistivities. They have a higher conductivity than dielectrics but a lower conductivity than conductors. The energy band gap of conductors (metals), semiconductors, and insulators is explained in Fig. 4. In contrast to metals, semiconductors exhibit insulating behavior at ambient temperature, but as the temperature rises, their electrical conductivity increases. It is possible to regulate the conductivity of semiconductors by adding appropriate impurities. Silicon, germanium, carbon, and so on are a few types of semiconductors. The fundamental component of contemporary electronics, semiconductors include transistors, solar cells, light-emitting diodes (LEDs), and digital and analog integrated circuits are examples of semiconductors. Modern knowledge of semiconductor properties is based on quantum physics, which describes how electrons and holes move within crystal structures and in lattices. Growing understanding of semiconductor materials and fabrication techniques has allowed for ongoing improvements in microprocessor complexity and speed.(10)

Adding impurity atoms to a semiconducting material, known as “doping” significantly raises the substance's charge carrier count. A doped semiconductor is referred to as "p-type" when it mostly consists of free holes, and "n-type" when it primarily consists of free electrons.(10)

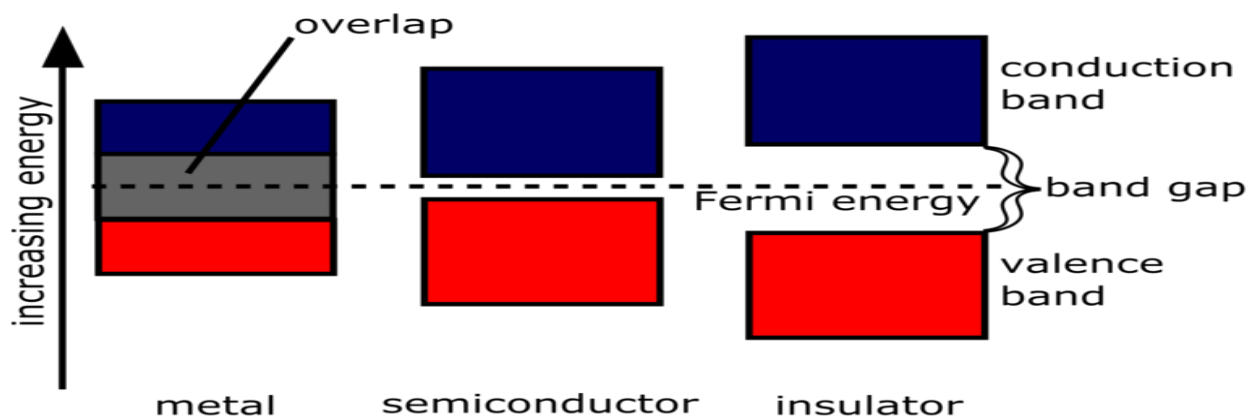


Figure 4 :Diagram representing the band theory of metals, semiconductors, and insulators

7.2. Band gap of semiconductor

Direct band-gap semiconductors are those in which the greatest valence band energy and the minimum conduction band energy occur at the same wave number or momentum. The electrical and

optical characteristics of a semiconductor is explained by direct band-gap materials. An energy greater than the band-gap must be supplied in order to elevate an electron from the valence band to the conduction band.(11)

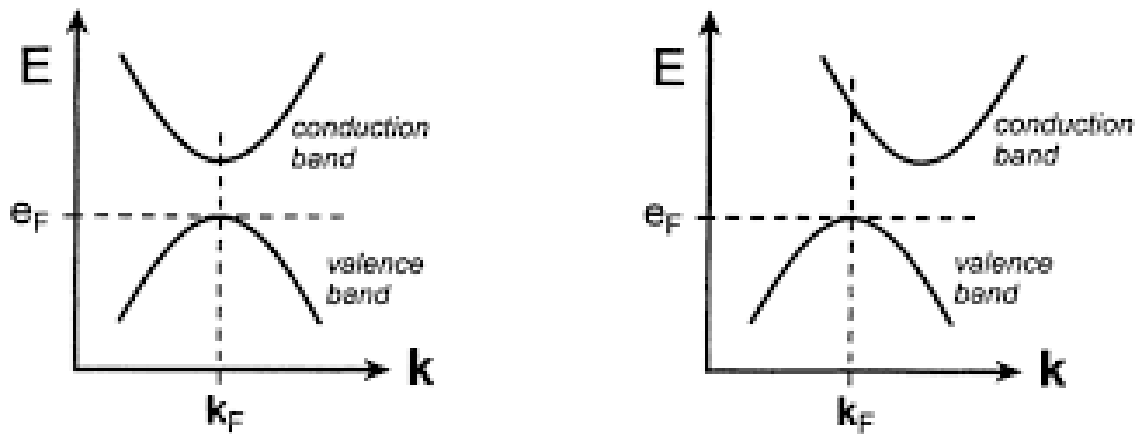


Figure 5 : direct band gap and indirect band gap semiconductor

In contrast to a direct band semiconductor, an indirect bandgap semiconductor is one in which the greatest valence band energy and the minimum conduction band energy occur at distinct wave number values or momentum.(11)

7.3. Classification of semiconductors.

Semiconductors may be classified broadly into intrinsic semiconductor and extrinsic semiconductor. Intrinsic semiconductors can also be referred to as pure or undoped elements (Si, Ge) whereas the extrinsic semiconductors are doped with other materials otherwise referred to as impurities and they can be n-type or p-type.

Intrinsic semiconductor

A semiconductor that is intrinsic as seen in Fig. 2, an intrinsic semiconductor is an extremely pure semiconductor material or one in which the number of holes in the conduction band equals the number of electrons. Such semiconductors have a very small forbidden energy gap, and the valence electrons may hop over to the conduction band using just the energy present at ambient temperature. The Fermi level of intrinsic semiconductors is located halfway between the valence and conduction bands, which

is another distinguishing characteristic of these materials. Electrons will gravitate toward the positive terminal and holes will gravitate toward the negative terminal if a potential difference is applied across an intrinsic semiconductor. The semiconductor's overall current.(10)

Extrinsic semiconductor

These are semiconductors where extremely small amounts of impurities are purposefully added to dilute the semiconductor material's pure condition. In comparison to inherent semiconductors, this improves their conductivity and characteristics. The impurities are referred to as doping agents or dopants. P-type or n-type semiconductors are created when dopants made of materials having three (trivalent) or five (pentavalent) electrons in their valence band are applied to a tetravalent base material (such as Ge). Only three electrons are donated by the trivalent atom, like B, to the tetravalent atom, leaving one hole unfilled. This is known as a p-type semiconductor because it produces more holes than electrons. Therefore, in p-type semiconductors, holes represent the bulk of the charge carriers.(10)

7.4. Binary nanoparticles

There are both metal and non-metal semiconductor nanoparticles in this collection. While the non-metals are mostly elements from early members of groups IV and V as well as elements from group VI, the metals are primarily the d-block elements, groups III, and lower members of groups IV and V. These comprise, among others, mercuric selenide (HgSe), cadmium selenide (CdSe), cadmium telluride (CdTe), zinc sulfide (ZnS), PbS, zinc oxide (ZnO), maghemite (γ -Fe₂O₃), magnetite (Fe₂O₃), GaN, TiO₂, SnS, and Bi₂Se₃.(10)

7.5. Chalcogenides nanoparticles

This class of semiconductor nanoparticles mostly consists of group IIIA, transition metals (excluding oxides) as anions, and lower members of IVA and VA as cations. Monochalcogenides (ZnS, ZnSe, CdSe, PbTe, PbSe, CdS, MoSe, CdSe, MnS, NiS, PdS, Cu₂S, NiS, ZnS, CdS, PbS, SnS), dichalcogenides (MoS₂, NiS₂, FeS₂, SnS₂), and trichalcogenides (M₂S₃; M = Bi, Sb, Ga, As) are possible categories. Because they resemble quantum dots, they exhibit strong edge and quantum confinement effects, indirect band gaps, outstanding stability, and good optoelectronic characteristics.(10)

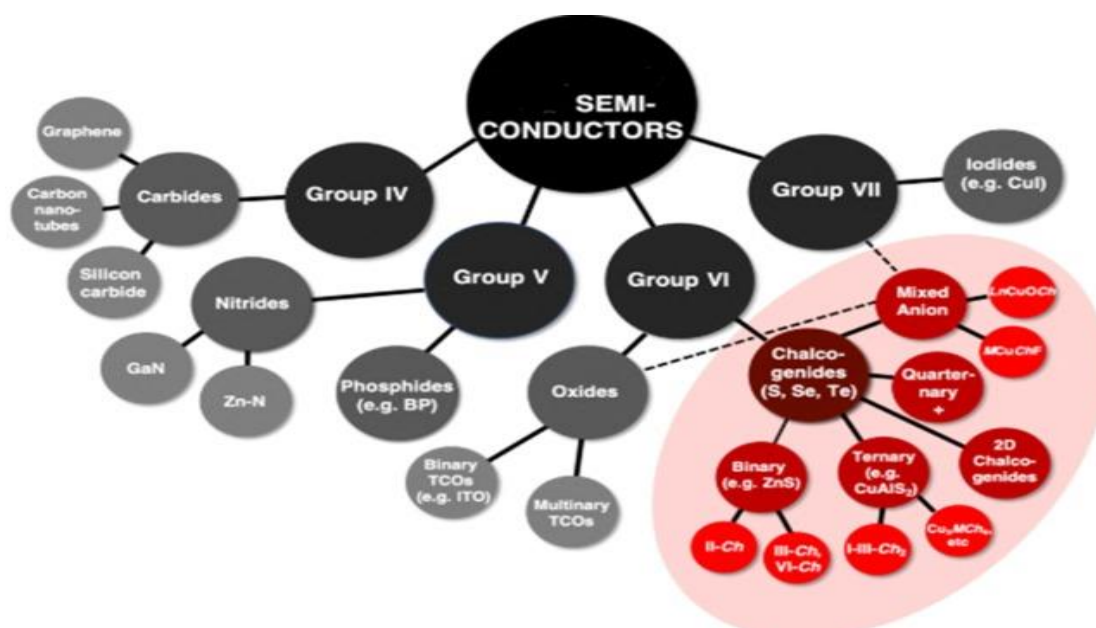


Figure 6 : Different types of semiconductor nanoparticles(10)

7.6. The semiconductor quantum dots

The first colloidal fluorescent semiconductor nanoscale crystals known as quantum dots were created in the early 1980s. Due to their distinct optical, electronic, and photophysical characteristics, these artificial semiconductor nanoparticles are often attractive for potential uses in solar cells, imaging, fluorescent biological labeling, composites, detection, and as effective donors of fluorescence resonance energy. Quantum confinement effects are present in sufficiently small semiconductor particles, limiting the energies at which electron-hole pairs can exist. Depending on the particle's size, its optical characteristics can be subtly altered based on the correlation between energy and light wavelength (or color). Consequently, distinct colored particles that emit or absorb certain light wavelengths can only be created by adjusting the size of quantum dots. Because of quantum confinement, various sized quantum dots produce different colors of light, as seen in Figure 1. Many of the characteristics seen naturally in atomic and nuclear physics of the quantum system are also found in the physics of quantum dots. (12)

Quantum confinement

The energy of confined electrons, which are not continuous in bulk materials like nanocrystals, is referred to as quantum confinement. The electrical, optical, and mechanical behavior of nanomaterials are impacted by these trapped electrons, which transform into a distinct set of energy levels. Because of their variable bandgap, quantum dots (QDs) are a novel family of materials that display quantum confinement features. In addition to being nanometer-sized semiconductor crystals, QDs also contain

tightly contained electrons or excitons. When nanomaterials are shrunk to fewer than 100-10 nm in size and form, the quantum confinement phenomenon takes place. It is essential to comprehend how bandgap may be adjusted in relation to size in order to comprehend how distinct energy levels and excitons develop.(13)

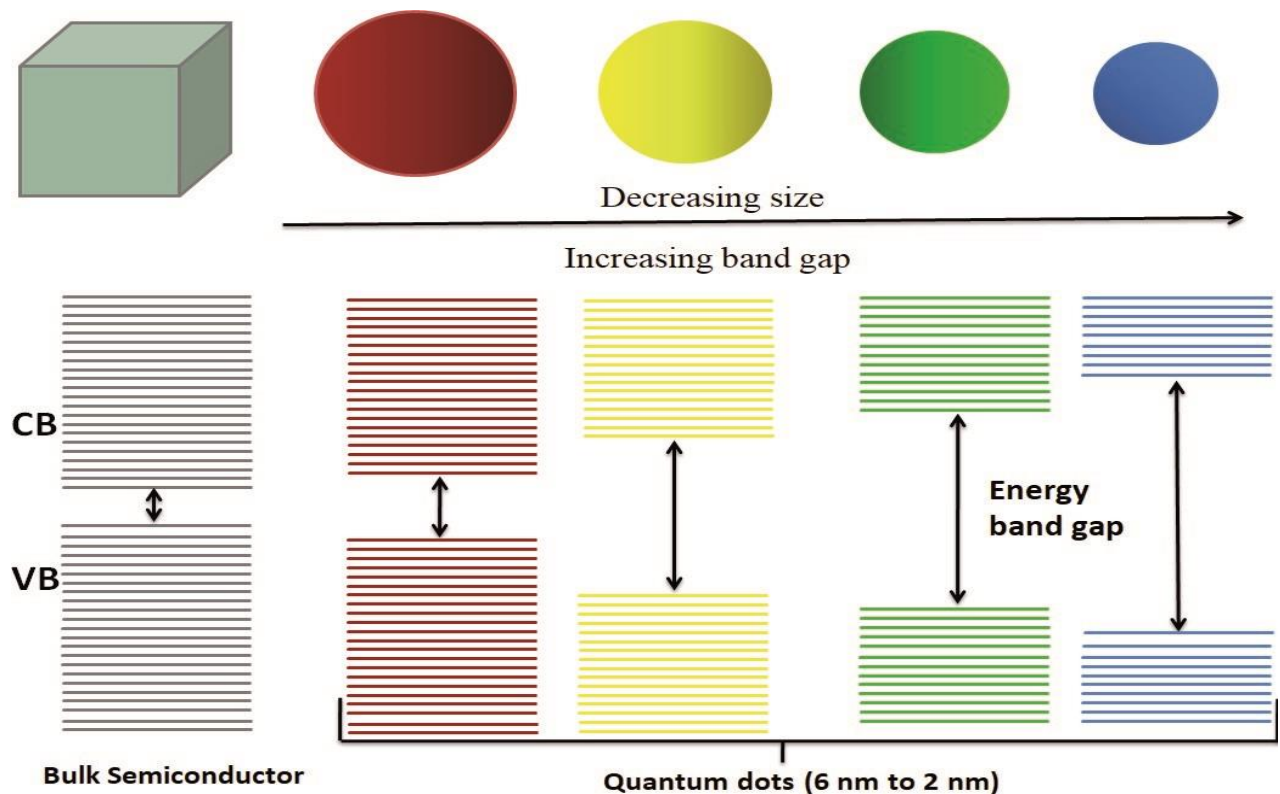


Figure 7 : Diagram showing energy band structures in atom ,bulk material and quantum nanostructure(13)

8. Tin sulfide

8.1. General information on tin sulfide

Binary compounds that are highly beneficial for optoelectronic devices may be found in the SnS system. Tin sulfide may form many phases, including SnS, SnS₂, and Sn₂S₃, due to the coordination properties of tin and sulfur. The most stable and intriguing materials for technology are tin Mon sulfide (SnS), tin disulfide (SnS₂), and the compounds (Sn₂S₃). (14) The nanostructures of GeS, SnS, and PbS are significant materials among the IV–VI group semiconductors. (15) Approximately 1.3 and 1.0 eV are the direct and indirect band gaps, respectively. (15)

| II | III | IV | V | VI |
|----|-----|----|----|----|
| | B | C | N | O |
| | Al | Si | P | S |
| Zn | Ga | Ge | As | Se |
| Cd | In | Sn | Sb | Te |

Table 1: Position of the elements Sn and S in the periodic table

8.2. The compound Tin (II) sulfide SnS

Semiconductors of the IV-VI group contain the chemical Tin (II) sulfide (SnS). In the realm of photovoltaics, binary SnS materials have advanced significantly. As a result, these SnS heterojunctions show intriguing structural, optical, and electrical properties. Their constituent elements Sn and S are abundant and are less toxic in nature.

8.3. properties of tin sulfide

Structural properties.

The SnS material mostly has two types of crystal structures: zinc blende and orthorhombic. SnS has an orthorhombic structure at room temperature, with two layers perpendicular to the Z-axis where weak Van der Waals interactions hold the Sn and S atoms together.(14)

Orthorhombic structure

The structure of SnS is made of six spherical atoms around the electron-hole pair, making a distorted octahedron. Three longer Sn-S bonds and three shorter ones with angles between 90° and 180° are seen. The stereochemical activity of the non-electronic pair is characterized by these deformations. The nearest atoms form a rectangular pyramid, and the structure may be thought of as a sequence of parallel helices. The leaves of SnS rely on the weak forces of Vander Waals to generate its orthorhombic structure.(17)

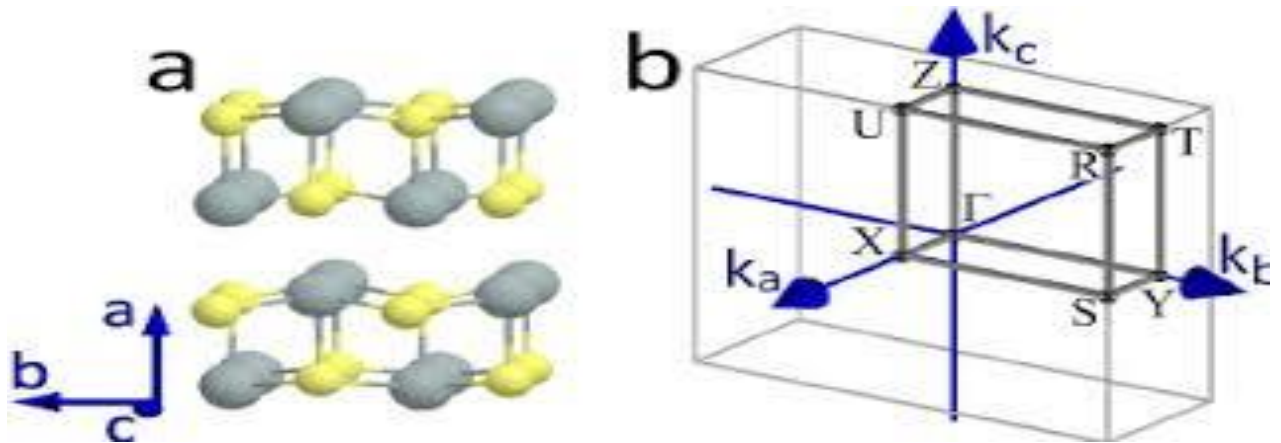


Figure 8 : Structural model of orthorhombic tin sulfide SnS(17)

Zinc blend structure

The sulfur ions S coordinate with the tin ions Sn in a tetrahedron in the zinc blende structure of the tin sulfide substance SnS.

The four vertices of this tetrahedral SnS₄ structure are shared by nearby tetrahedra.

We can see from these two structures that the zinc blende structure is more compact and tougher than the orthorhombic one.

There are several different phases of tin sulfide, but SnS is the most stable, practical, and widespread.

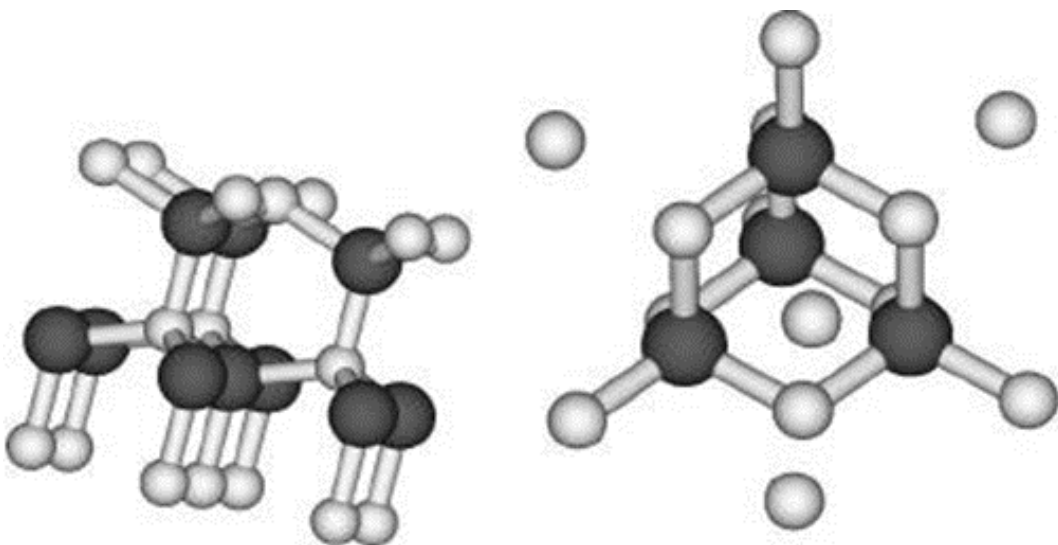


Figure 9 : Elementary cell of the zinc blend structure

8.4. Optical properties

Transmission

Tin sulfide SnS thin films can be used as an absorber material in photovoltaic cells because of its low transmittance in the visible portion of the solar spectrum, which is between 400 and 800 nm.

The optical gap and absorption coefficient of SnS

in sulfide (SnS) is a semiconductor with both an indirect band gap of 1.1 eV and a direct band gap of 1.2 eV. It has a notably high absorption coefficient, particularly above its band gap. Figure 8 illustrates the absorption spectra for two SnS structures: orthorhombic and zinc blende. In the visible and near-infrared regions, SnS shows a direct transition with an absorption coefficient exceeding 10^5cm^{-1} . The orthorhombic structure of SnS exhibits significant absorption starting at 980 nm due to its direct band gap, while its indirect band gap leads to a lower absorption limit near 1100 nm. In contrast, the zinc blende structure of SnS displays distinct absorption, with strong absorption occurring at approximately 700 nm.

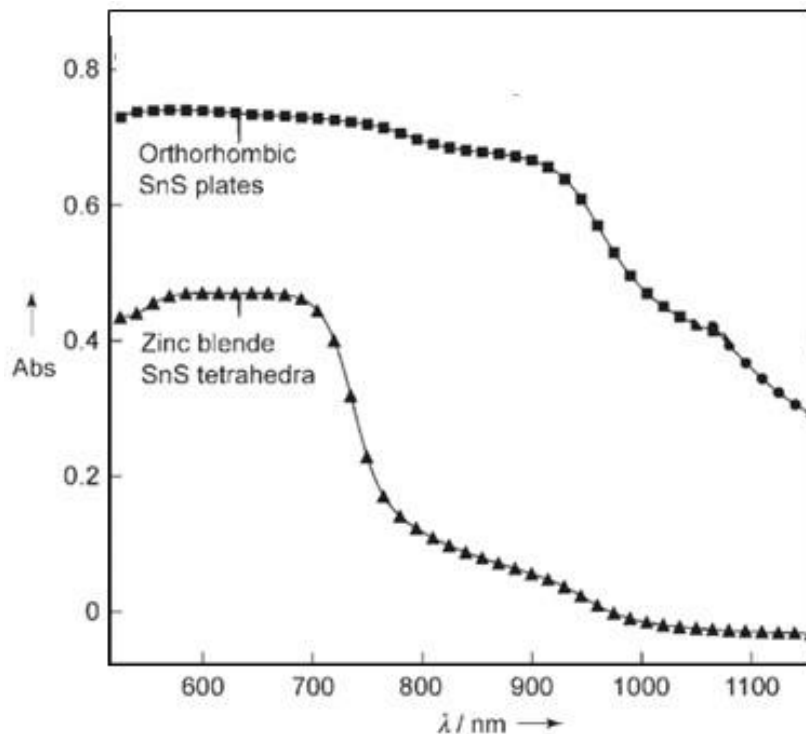


Figure 10 : Absorption spectra for the tin sulfide SnS nanoparticles(16)

SnS is a IV–VI semiconductor and its optical properties are of interest because of its several optoelectronic applications, such as holographic recording, near-infrared detector, solar absorber and the Hall

effect. A material's optical properties depend on the optical band edge, which can vary with changes in shape, size, strain, doping and surface modifications.

8.5. Electrical properties

In recent years, tin sulfide (SnS) has garnered a lot of interest due to its electrical characteristics. The electrical characteristics of this material have been the subject of several investigations with the goal of improving them. In the dark, SnS films' electrical resistivity typically falls between 10^5 and 10^6 Ωcm (for the orthorhombic structure and without annealing). Additionally, SnS films and zinc blende (without annealing) have an electrical resistance of around 1.7×10^7 Ωcm in the dark. It is widely acknowledged that excessive electrical resistance is not advantageous for use in solar cells.(18)

However, there are thin-film fabrication techniques that have demonstrated they can prepare SnS films with a dark resistivity as low as that theoretically studied. Additionally, this can be very helpful for creating inexpensive solar cells with SnS as the light-absorbing layer. Moreover, SnS exhibits both p-type and n-type conductivity . (18)

A large concentration of flaws in the formed crystal may be the cause of the sharp decline in the observed mobility value. The defect scattering mechanism also restricts carrier mobility. The increased dispersion brought on by the flaws significantly reduces mobility and shortens the carrier life time(19). **Fig. 10** displays the electrical band structure of SnS as computed. SnS has a direct electronic band gap of 1.22 eV and a spatially indirect fundamental electronic band gap of 1.11 eV. Low transition intensities in the SE data prevent it from being resolved, but the indirect gap prediction at 1.11 eV is in line with findings from earlier theoretical and experimental investigations.(20)

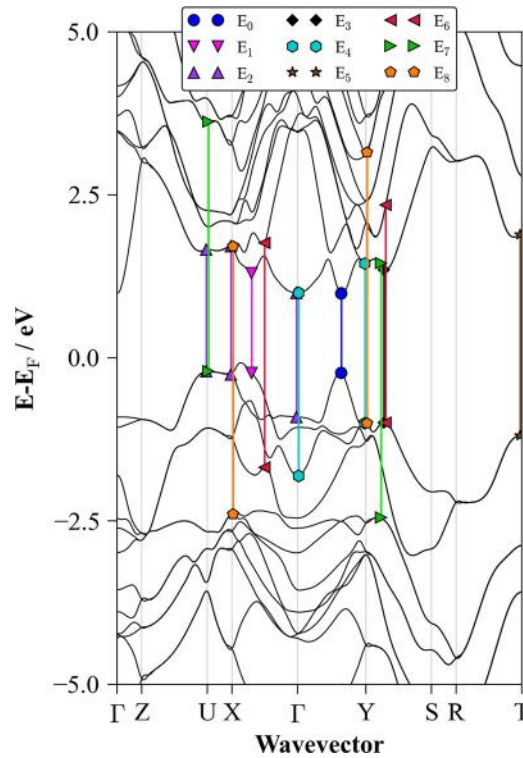


Figure 11 : The calculated electronic energy band structure of SnS(20)

8.6. Application of Tin sulfide

Because of its special qualities, such as its direct band gap, high absorbability, tunable electrical properties, thermal and chemical stability, and layered structure, SnS semiconductor has the potential to be a valuable material for a range of applications, including photovoltaics, optoelectronics, chemical sensors, solid-state batteries, holographic, etc(21)

Photovoltaic application

because of its strong absorption and small band gap, SnS gained attention as a potential material for solar cell systems. In this regard, a range of photovoltaic devices have been made by employing various n-type materials as window layers and p-SnS films as absorber layers.(21) Solar cell production has also made use of SnS. Lithium-ion batteries and other energy storage devices have been successfully developed using SnS.(22)

Other applications

Catalysis is another area where SnS finds use. because of its favorable band alignment and strong photoresponse, SnS is regarded as an efficient hydrogen evolution catalyst.(22) Additionally, SnS has been utilized in the development of several chemical detectors for use in the biomedical, environmental protection, and safety domains.(22)

Tin sulfide (SnS) also finds application in solid-state batteries, which have recently garnered significant interest due to their enhanced dependability and safety, particularly those incorporating a solid electrolyte (21). Furthermore, SnS has been utilized in the development of transistors and other electronic devices, as demonstrated by Sucharitakul et al. Beyond these, SnS is employed in sensors for detecting various volatile organic compounds, including methanol, ethanol, acetone, and 1-butanol, showcasing its utility in air sensing applications (22).

Toxicity

There are exciting new prospects for the development of the construction sector thanks to the science of nanotechnology. However, because of the wear and disposal of building materials that include nanoparticles, workers and consumers are at extremely high risk for health problems. The toxicity of nanoparticles is caused by molecular mechanisms that include the production of reactive oxygen species (ROS), oxidative stress, inflammation, damage to cell organelles and DNA, protein denaturation, and impairment of cell metabolism. Because of their small size, nanoparticles can enter key organs like the stomach and lungs or be swallowed, and they can then go to secondary organs. Inhaling nanoparticles can cause immediate or long-term chronic diseases, as well as systemic effects. Numerous studies demonstrate a connection between respiratory and cardiovascular disorders and nanoparticle exposure.

Conclusion

This chapter has provided a comprehensive introduction to the rapidly evolving fields of nanoscience and nanotechnology, highlighting the unique properties of nanostructured materials, particularly semiconductors, at the atomic scale. We distinguished between nanoscience as the study of nanoscale phenomena and nanotechnology as its practical application. The discussion also covered various types of nanoparticles, their classifications (organic and inorganic), and the prevalent synthesis methods, emphasizing the advantages of bottom-up chemical approaches like the hydrothermal method chosen for this research.

A significant portion of the chapter was dedicated to semiconductor nanoparticles, detailing their fundamental properties, including band gap theory (direct and indirect) and classification into intrinsic and extrinsic types. Special attention was given to binary and chalcogenide nanoparticles, leading to an in-depth examination of tin sulfide (SnS). We explored its structural properties (orthorhombic and zinc blende phases), optical characteristics such as high absorption coefficient and suitable band gaps for photovoltaic applications, and electrical properties, noting its potential for low resistivity. Finally, the diverse applications of SnS were highlighted, particularly in photovoltaics, catalysis, and sensing, while also acknowledging the critical aspect of nanoparticle toxicity and associated health risks. This foundational understanding sets the stage for the experimental work aimed at synthesizing and characterizing Fe^{2+} and Cu^{2+} doped SnS nanoparticles for enhanced optical and photocatalytic performance.

Chapter II synthesis and characterization

1. SYNTHESIS

1.1. INTRODUCTION

Through the manipulation of synthesis conditions, the hydrothermal synthesis method is a highly effective approach for adjusting the morphology of a synthesized sample. The unique qualities needed for certain applications were found to be greatly enhanced by various morphologies. Two sections make up the general reaction mechanism of hydrothermal synthesis. A precursor must first dissolve in a certain solvent in order to convert the starting material into ions. The final product is achieved by the second phase, crystallization, which takes place at a supersaturated state (maximum solubility of precursor) and facilitates both nucleation and particle growth. (23)

The word "hydrothermal" has only geological roots. The British geologist Sir Roderick Murchison (1792–1871) was the first to utilize it to explain how water at high temperatures and pressures causes changes in the earth's crust that result in the production of different rocks and minerals.(24)

This method is easy to use, non-polluting, and energy-efficient. The hydrothermal synthesis process has a number of important benefits over other methods(25) and it was chosen to produce SnS NPs.

1.2. Hydrothermal synthesis

1.2.1. PRINCIPLE

One of the most popular techniques for creating nanomaterials is hydrothermal synthesis. In essence, it is a solution-reaction-based methodology. The creation of nanomaterials via hydrothermal synthesis can occur at temperatures ranging from ambient temperature to extremely high temperatures. Depending on the vapor pressure of the primary composition in the reaction, either low-pressure or high-pressure conditions can be utilized to regulate the morphology of the materials to be synthesized. This method has been successfully used to create a wide variety of nanomaterials.(25)

Reactants are heated using the hydrothermal technique in a closed vessel known as an autoclave while water is present. The superheated water stays liquid above its boiling point, surpassing air pressure, while the pressure rises during heating. We can lessen the quantity of harmful materials and organic solvents by using water as a solvent. Utilize This method's benefit is that it uses less energy because of its low temperatures. At the molecular level, a homogenous mixture (colloidal solution) of precursors is produced in the solution.(5)

1.2.2. EQUIPMENT

An autoclave, which is defined as a cylindrical cylinder with enough volume to hold the precursors and solvents, is the crystallization apparatus utilized. Previously, they were added to a Teflon® reactor, which is made of polytetrafluoroethylene and slides into the autoclave. The envelope of the autoclave is constructed of stainless steel and needs to be inert to the solvent. To ensure that the entire system can tolerate the increase in temperature and pressure, the autoclave's seal is crucial. Numerous models have been created.(26)

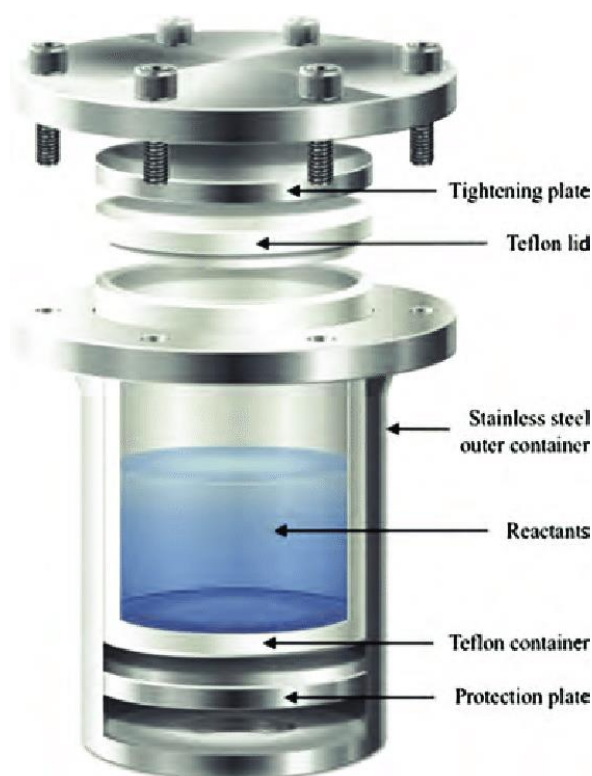


Figure 12stainless steel autoclave(27)

1.2.3. EXPERIMENTAL PROTOCOL

The following is a description of the experimental procedure utilized to synthesize the investigated NPs:

- the chemical salts in as little water as possible, keeping in mind that the solution's volumetric capacity cannot be greater than two-thirds ($2/3$) of the container's volume.
- The selection of the reaction media, including temperature, pH, and concentration.

- A Teflon reactor is filled with the prepared reaction mixture. After that, it is placed into an autoclave made of stainless steel.

For a specified amount of time and at a specific temperature, the autoclave is placed in an oven.

1.3. Synthesis of tin Sulfide nanoparticles

The objective of the synthesis is to obtain: - a pure phase – a good yield Exact amounts of raw materials are necessary to synthesis pure and doped SnS nanoparticles, and the main raw materials used are tin chloride [$\text{Sn Cl}_2 \cdot 2(\text{H}_2\text{O})$] and thiourea [$\text{SC}(\text{NH}_2)_2$], which are sources of tin ions (Sn^{2+}) and sulfide ions (S^{2-}), respectively

By properly regulating the stoichiometry and reaction parameters, such as temperature, pressure, and reaction time, it is possible to adjust the characteristics of the produced SnS nanoparticles, including their size, shape, and doping level.



Figure 13 : synthesis protocol

1.3.1. Pure SnS

Pure and doped SnS nanoparticles are synthesized using the following experimental protocol:

- ✓ Dissolve 2.8g of tin chloride [$\text{SnCl}_2 \cdot 2(\text{H}_2\text{O})$] in 25ml of distilled water in a beaker.
- ✓ In another beaker, homogenize 1.1g of Thiourea [$\text{SC}(\text{NH}_2)_2$] in 25ml of distilled water.
- ✓ For 30 minutes, mix the tin chloride solution with a magnetic stirrer while adding the Thiourea solution dropwise.
- ✓ Move the mixture into a container made of PTFE.
- ✓ Put the jar of PTFE into an autoclave.
- ✓ Subject the autoclave to a temperature of 180°C for 8 hours.
- ✓ Use an oven to carry out the reaction.



Figure 14 : Phase of pure SnS nanoparticle synthesis

By applying high temperatures and pressures, an autoclave facilitates the hydrothermal process and encourages the production of distinct nanoparticles.



Figure 15 : Phase of pure SnS nanoparticle synthesis

1.3.2. Doped SnS

Synthesis of Fe-doped NPs

The following steps were taken in order to create Sn^{2+} doped ZnS nanoparticles with the formula $\text{Sn}_{(1-x)}\text{Fe}_x\text{S}$, which is represented as SnS: x% Fe. Dropwise add an x mmol solution of $\text{FeCl}_2 \cdot 2\text{H}_2\text{O}$ in 5 mL H_2O to a solution of (1-x) mol tin chloride in 25 mL H_2O while stirring continuously for 10 minutes to create a mixed Sn/Fe solution.

using solution mixing, add Thiourea solution, stir magnetically, move to a PTFE container, and then place in the autoclave, using the same procedure as for the production of non-doped SnS nanoparticles.

Set the autoclave to the specified temperature and time in accordance with the hydrothermal synthesis parameters for SnS nanoparticles that are not doped.

| Dopant percentage | Mass of Iron chloride |
|-------------------|-----------------------|
| SnS doped 1% Fe | 30 mg |

Table 2: Mass of Iron chloride as a function of the percentage of dopant

Synthesis of Cu-doped NPs

Cu-doped SnS nanoparticles are synthesized following the same procedure as for undoped SnS nanoparticles, with the sole modification being the substitution of the pure tin chloride solution with a solution containing copper chloride.

| Dopant percentage | Mass of Cooper chloride |
|-------------------|-------------------------|
| SnS doped 1% Cu | 20,16 mg |

Table 3 : Mass of Iron chloride as a function of the percentage of dopant

Synthesis of Fe and Cu co-doped NPs

Using the same processes as previously outlined for SnS nanoparticles Fe-Cu co-doped SnS nanoparticles are created by substituting a solution containing both iron chloride and cooper chloride for the pure tin chloride solution.

| Dopant percentage | Mass of co-dopant |
|----------------------|--------------------------------|
| SnS doped 1% Cu 1%Fe | 30 mg of Fe and 20,16 mg of Cu |

Table 4: Mass of iron chloride as a function of the percentage of dopant



Figure 16 : components of doping

After their synthesis, both pure and doped ZnS nanoparticles undergo a thorough cleaning process to remove impurities and residual reactants. This multi-step washing procedure involves sequential rinses with various solvents, ensuring high purity.

1.3.3. Washing Procedure

Distilled Water Rinse: Nanoparticles are first rinsed with distilled water to eliminate water-soluble contaminants and remaining reactants. This step is repeated multiple times, separating the nanoparticles from the washing solution via centrifugation or filtration after each rinse.

Ethanol Rinse: Following the water wash, nanoparticles are rinsed with ethanol to remove organic impurities and residual solvents. Similar to the water rinse, nanoparticles are separated from the ethanol solution, and this step is repeated as needed.

Acetone Rinse: An acetone rinse targets any lingering organic contaminants, including oils and greases. This powerful solvent ensures a more complete removal of such impurities, with the rinsing process repeated several times for thorough cleaning.

Methanol Rinse: Finally, the nanoparticles are cleaned with methanol to ensure the complete elimination of any remaining solvents and final traces of contaminants. The nanoparticles are separated from the methanol solution, and this step can be repeated if necessary.

Drying and Further Processing

Once the washing is complete, the nanoparticles are typically dried in a desiccator or under vacuum to remove any residual solvent. After this purification process, the cleaned nanoparticles are ready for further analysis or various applications.



Figure 17 : Hanging and washing

Unlike the undoped component, colorful compounds are generated during autoclaving. Visually, this coloring shift is noticeable, and we can see that the degree of doping affects the coloration's intensity. Figure II.5 shows this phenomenon, where the doping concentration is correlated with the color intensity of the produced chemicals.


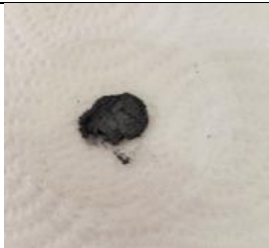


| Sample | SnS | SnS 1% Fe | SnS 1% Cu | SnS 1%Fe 1%Cu |
|--------|---|---|--|---|
| Color |  |  |  |  |

Figure 18 : pure and doped SnS powders after drying

2. Characterization

The characterisation methods used to identify our SnS powders are listed below, along with the corresponding outcomes.

2.1. X-ray Diffraction (XRD)

XRD analysis was conducted to determine the crystalline structure and phase purity of the SnS powders. The results revealed the presence of characteristic peaks corresponding to the orthorhombic phases of SnS, confirming the crystallinity of the synthesized powders. In fact, one of the best techniques for describing the structure of nanopowders is X-ray diffraction (XRD). It offers important information on the purity, phase composition, and crystalline structure of the produced powders. The capacity of XRD to examine the diffraction patterns produced when X-rays contact with the material's crystallographic planes accounts for its efficacy.

Overall, XRD plays a crucial role in verifying the formation of desired nano powders and assessing their purity, providing essential information for understanding the structural properties of nanomaterials and their potential applications.

It is well-established that Tin sulfide (SnS) crystallize in orthorhombic forms. X-ray diffraction (XRD) spectra provide valuable information about the crystallographic structure of materials, including the identification of specific crystallographic planes

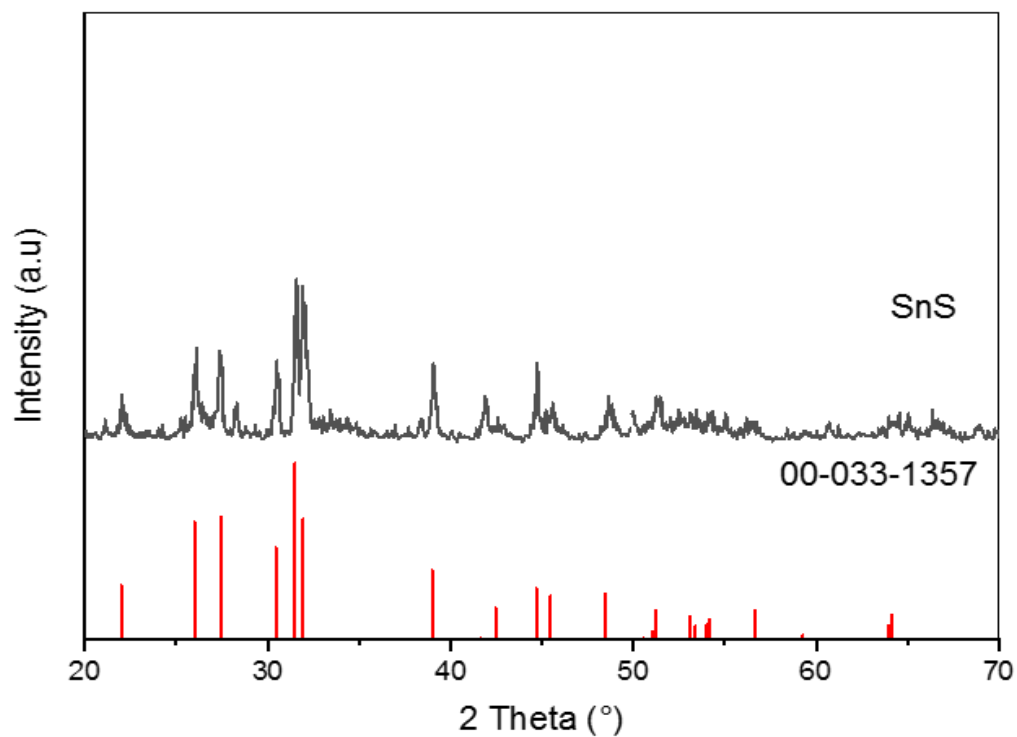


Figure 19 : comparison of the spectrum of non-doped SnS NPs with the ICOD

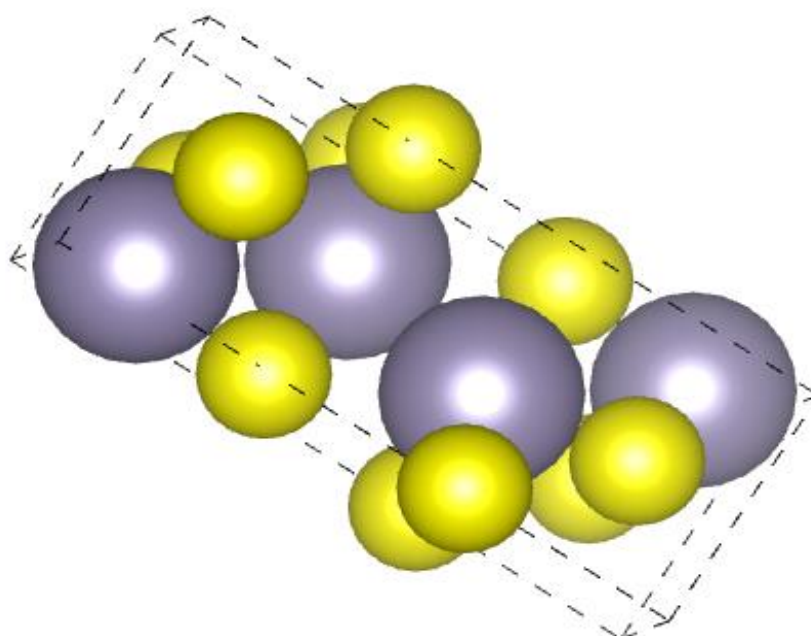


Figure 20 : Tin sulfide structure drawn by vesta win 64

There are several and strong peaks in the XRD spectra. Peak locations were in good agreement with the standard ICOD card no. 00-033-1375, and the strong and crisp diffraction peaks indicate that the synthesized SnS samples were well-crystallized. Single-phase tin monosulphide production is implied by the lack of distinctive peaks of impurities such as metal tin, SnS₂, and SnO₂. The crystallite size was estimated to be 22,12 nm

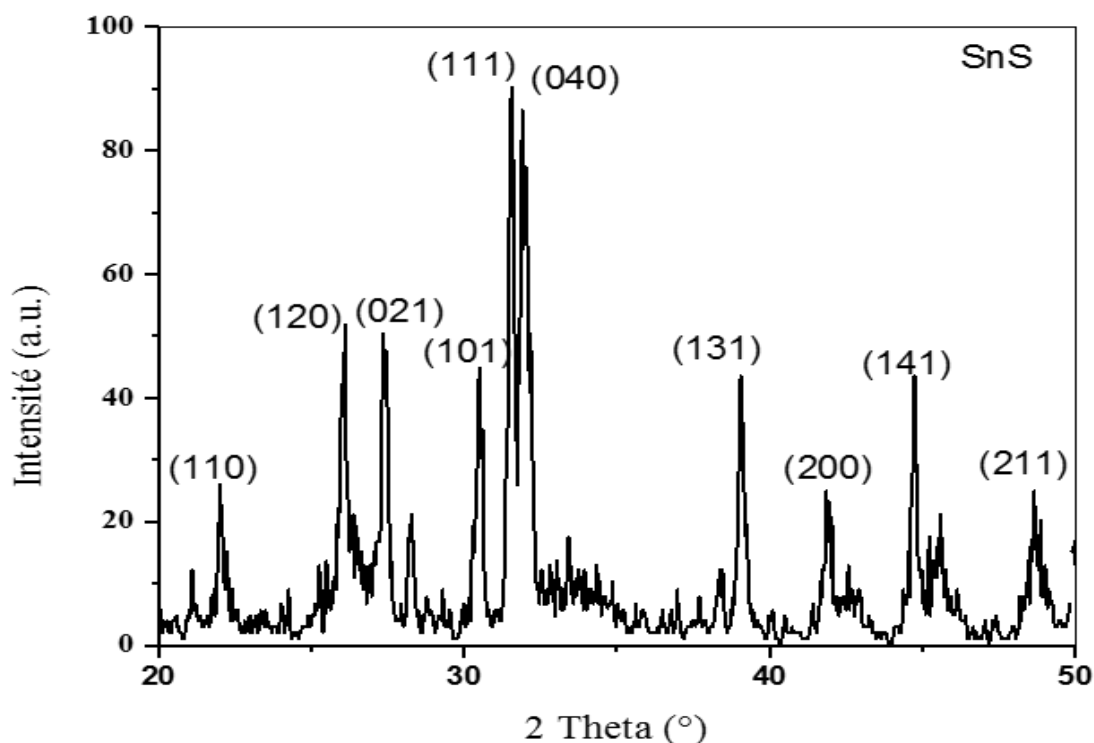


Figure 21 : XRD of pure SnS

Analysis of the spectra allows us to observe peaks at angular positions $2\theta = 21.97^\circ, 25.97^\circ, 27.43^\circ, 30.44^\circ, 31.49^\circ, 31.93^\circ, 39.01^\circ, 41.66^\circ, 44.69^\circ$ and 48.48° corresponding to the Bragg planes (hkl) of (110), (120), (021), (101), (111), (040), (131), (200), (141) and (211) which corresponds to the orthorhombic SnS. This consistency validates the structural identification of the synthesized SnS samples.

2.1.1. Doping effect

SnS :1% Cu

The result, shown in *figure22*, revealed many distinct diffraction peaks located at 2θ values of $21.97^\circ, 25.97^\circ, 27.43^\circ, 30.44^\circ, 31.49^\circ, 31.93^\circ, 39.01^\circ, 41.66^\circ, 44.69^\circ$ and 48.48° , these peaks correspond to the (110), (120), (021), (101), (111), (040), (131), (200), (141) and (211) lattice planes, respectively, of the orthorhombic crystalline phase of SnS.

Crucially, the XRD spectra showed no new Fe- or FeS-related peaks, suggesting that Fe had effectively replaced Sn in the SnS host lattice. The SnS lattice structure's Fe doping is confirmed by this discovery. it is observed from the diffraction peaks are almost the same but the relative intensity of the peaks increases slightly upon Fe^{2+} ions doping.

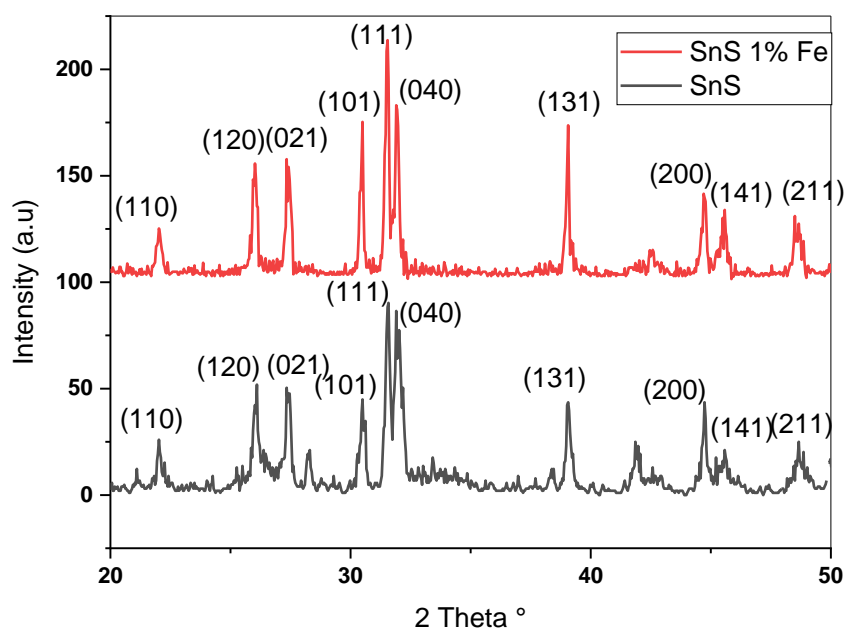


Figure 22 : COMPARISON OF THE SPECTRUM OF NON-DOPED and Fe-doped SnS NPs

SnS :1% Cu

The results are presented in **fig 23**. The diffraction peaks were indexed as (110), (120), (021), (101), (111), (040), (131), (200), (141) and (211) for the crystallographic planes observed at the angular

position $21.97^\circ, 25.97^\circ, 27.43^\circ, 30.44^\circ, 31.49^\circ, 31.93^\circ, 39.01^\circ, 41.66^\circ, 44.69^\circ$ and 48.48° of the orthorhombic crystalline phases of SnS.

Notably, no additional peak corresponding to the binary system CuS or Cu impurity was observed in the XRD patterns, indicating the presence of a single phase Cu:SnS compound. This confirms the substitution of Sn by Cu in the SnS lattice structure without the formation of separate phases.

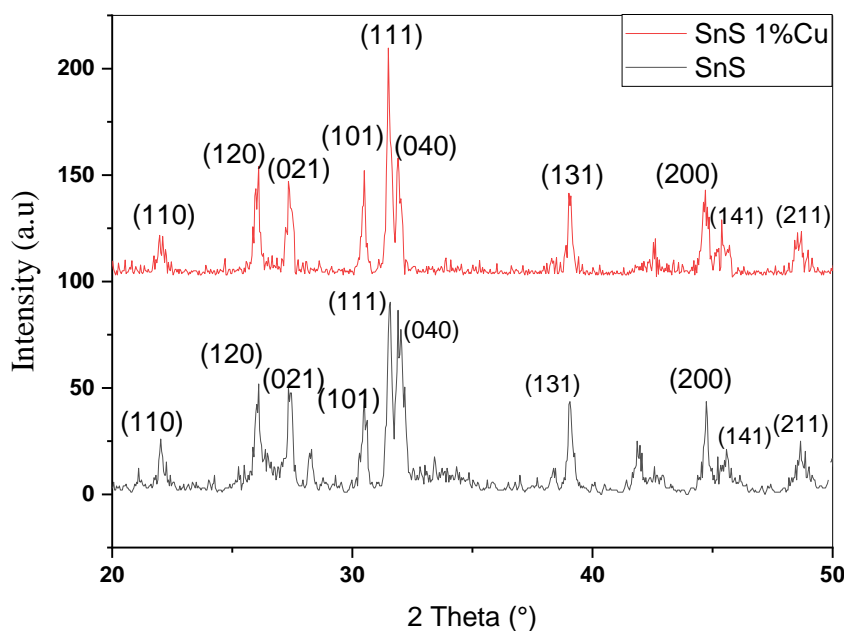


Figure 23 : comparison of the spectrum of non-doped and Cu- doped SnS NPs

Hence the observed shift in 2θ peak position can be related with the difference in ionic radius between Sn^{2+} (1.22\AA) and the dopant cation Cu^{2+} (0.73\AA)

The observation of the SnS:Cu nanoparticles' single-phase nature and the lack of impurity peaks validate the high purity and successful synthesis of the doped SnS samples. These findings demonstrate the structural changes brought about by Pb doping in SnS and offer important insights into how doping affects material properties.

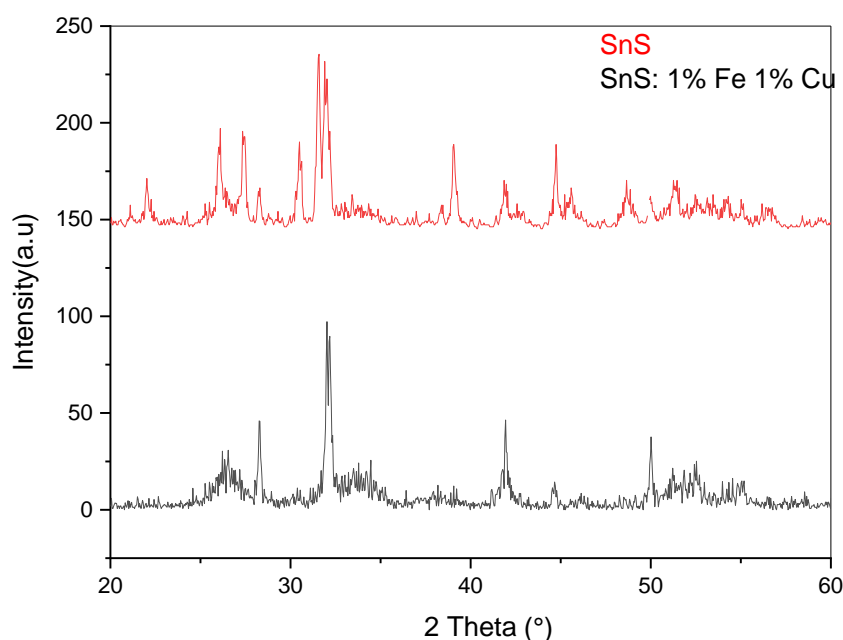


Figure 24 : comparison of the spectrum of non-doped and co-doped SnS

Overall, the XRD study highlights the different behaviors of Fe^{2+} and Cu^{2+} ions in the crystal lattice and offers more proof of the produced nanoparticles' purity. It also sheds light on the doping mechanisms of these ions in SnS. Grain size and lattice parameter values may be computed by using the Debye-Scherrer equation on the XRD data. These values offer important information about the structural characteristics of the produced nanoparticles. After obtaining the pertinent parameters, they may be combined into Table II.4 for additional comparison and analysis. The size and lattice properties of the manufactured nanoparticles may be well understood thanks to this collection, which facilitates the interpretation of their structural features and their uses.

| Sample | Grain size(nm) |
|-------------------|----------------|
| SnS | 22,12 |
| SnS:1%Fe | 28,93 |
| SnS:1%Cu | 24,16 |
| SnS:1%Fe and 1%Cu | 31,3 |

Table 5: Grain size and lattice parameter of undoped and doped SnS NPs

When Fe and Cu dopants are added, the SnS lattice's empty zinc sites are filled, which results in the grain size increase that has been observed. The presence of Fe and Sn ions in these empty spaces decreases the likelihood of structural flaws and improves the material's overall crystallinity, which results in bigger grain sizes.

2.2. Fourier Transform Infrared Spectroscopy (FTIR)

FTIR spectroscopy was employed to analyze the chemical bonding and functional groups present in the SnS powders. The spectra obtained showed characteristic absorption bands corresponding to Sn-S bonds, confirming the formation of SnS.

FT-IR analysis

One effective analytical method for identifying organic, polymeric, and occasionally inorganic compounds is Fourier Transform Infrared Spectroscopy, often known as FTIR Analysis or FTIR Spectroscopy. FTIR analysis offers important information on the composition and structure of materials by examining the functional groups found in a compound, molecular geometry, and intramolecular or intermolecular interactions.

The FTIR spectra of the samples were recorded at ambient temperature in order to examine the structural characteristics and functional groups of undoped and Fe, Cu, and Fe-Cu doped SnS NPs. The figure shows the FTIR spectra, which span the wavenumber range of 4000 to 400 cm^{-1} .

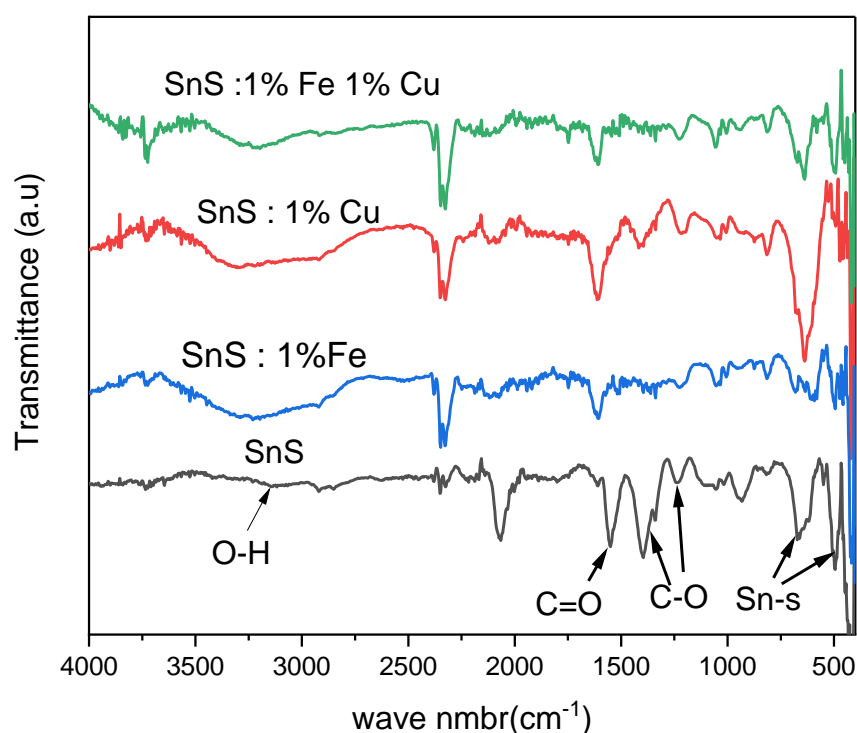


Figure 25 : FTIR spectra of the undoped and Fe,Cu and Fe and Cu SnS NPs

The FTIR plot shows four curves-pure SnS, SnS with 1% Fe, SnS with 1% Cu, and SnS with both metals-so lets walk through what each feature means. Around 3400 cm^{-1} a broad peak appears in every trace. This O-H band signals adsorbed water or hydroxyls on the nanoparticle surface, and its presence in all samples after synthesis hints that some moisture survives the drying steps. Three weaker bands stand out near 1600 , 1400 , and 1100 cm^{-1} . The peak near 1600 cm^{-1} probably arises from the C=O stretch of carboxyl groups, possibly left over from carbonates or organics used during synthesis. The features between 1400 and 1100 cm^{-1} could be C-O stretching or O-H bending, pointing to light organic residue or surfactant ligands that washing did not entirely remove.

Moving to lower energies, the key Sn-S signature appears below 600 cm^{-1} . There, two sharper peaks confirm the presence of SnS in all four samples. The close match between the bands of pure and doped materials implies that adding Fe or Cu leaves the Sn-S link in the lattice unchanged, a point already backed by the XRD data.

Effect of doping (Fe and Cu): Looking at the spectra, the curves for the doped particles (SnS:1%Fe, SnS:1%Cu, SnS:1%Fe 1%Cu) stay so close to pure SnS that we must conclude doping leaves no visible mark in this measurement.

2.3. Thermal analysis

Analysis of Heat Thermal treatment can alter a substance's physicochemical characteristics, including volume fluctuation, oxidation, pyrolysis, breakdown, phase shift, and structural alteration. We can see these changes as a function of temperature thanks to thermal analysis. Thermogravimetric analysis (TGA) and differential thermal analysis (DTA) are two of the methods used. The mass fluctuation of a sample as a function of the temperature at which it is thermally treated can be measured using a thermal analysis technique called thermogravimetric analysis. This change in mass may be a mass loss, like vapor emissions. Using the weight change that results from heating a sample at a steady pace, this method assesses a material's thermal stability.(28)

Analysis of Differential Heat (DTA) The technique involves calculating the temperature differential (ΔT) between the sample under study and an inert reference sample that is heated at the same pace. The quantity of heat that the substance under study releases or absorbs is connected to this discrepancy. Thus, we document ΔT as a temperature function. This makes it possible to identify peaks in both exothermic and endothermic reactions.(28)

ATG and ATD analysis

Thermal gravimetric analysis (TGA) consists of recording mass variations during a thermal cycle related to chemical reactions or departures of volatile constituents adsorbed or combined in a material.

The temperatures at which these mass losses occur constitute additional information to that obtained by DTA. For the identification of the physicochemical phenomena involved, the two characterizations are often carried out simultaneously in the same device.

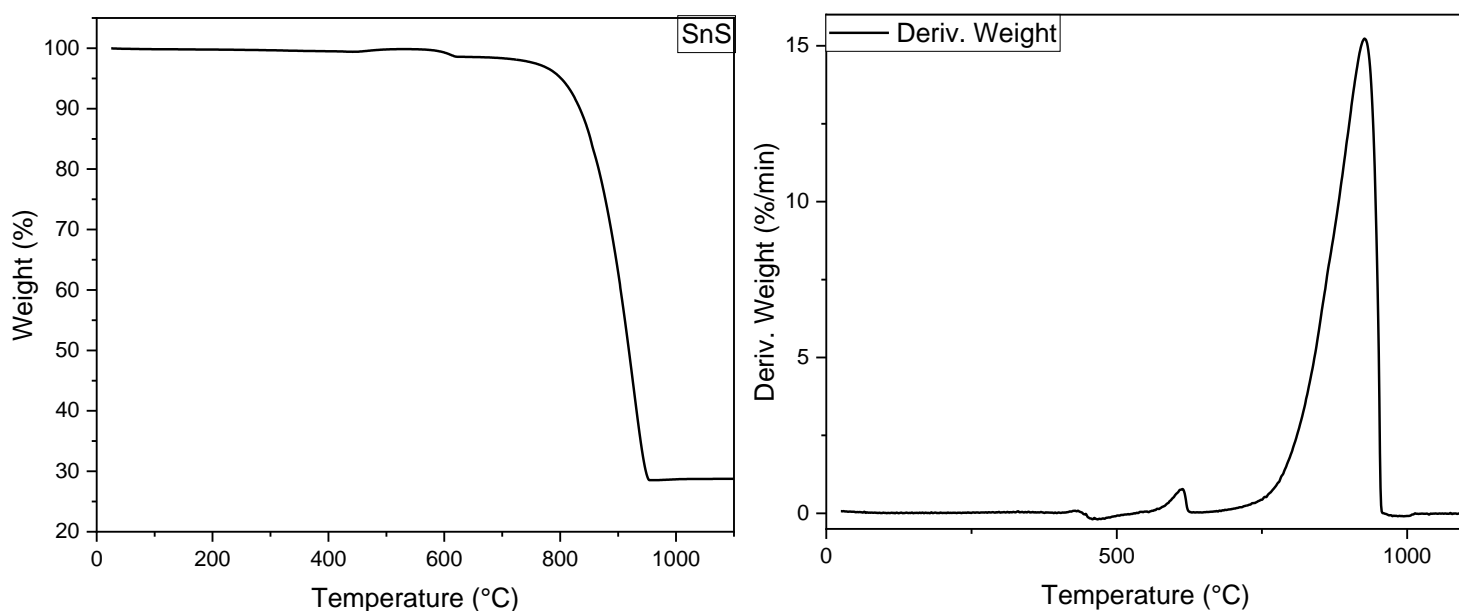


Figure 26 : TGA and DTA analysis

Figure 26 shows the combined analysis of TGA and DTA curves provides a more comprehensive view of the thermal transformations of SnS nanoparticles.

Initial Stability (0 °C - approximately 550 °C):

- **TGA:** Minimal mass loss (< 1%), indicating stability.
- **DTA:** No significant peaks, confirming the absence of major transformations.

SnS nanoparticles are thermally stable in this range. The small TGA fluctuation around 100 °C (moisture/residual solvents) is not accompanied by a strong DTA signal, as these processes have low enthalpy.

First Transition (approximately 550 °C - 750 °C):

- **TGA:** Slight mass loss (from 99% to 97%), potentially related to organic residues or non-stoichiometric sulfur compounds.
- **DTA:** A small exothermic peak (around 600 °C).

The low mass loss in TGA is associated with an exothermic event in DTA. This could suggest crystallization or minor oxidation/decomposition of surface residues that release energy.

Main Decomposition (approximately 750 °C - 950 °C):

- **TGA:** Major and rapid mass loss (from 97% to 28-29%), indicating the decomposition of SnS nanoparticles.
- **DTA:** A large and intense exothermic peak (culminating around 900-920 °C).

The massive decomposition of SnS nanoparticles is a highly exothermic process. This strengthens the hypothesis of an oxidation reaction or another decomposition process that releases energy, rather than a simple volatilization or an endothermic process. The significant mass loss (approximately 68-69%) indicates the volatilization of certain decomposition products, probably sulfur as SO₂. The residue (approximately 28-29%) is likely tin oxide (SnO₂). $\text{SnS} + \text{O}_2 \rightarrow \text{SnO}_2 + \text{SO}_2$

Final Plateau (above 950 °C):

- o **TGA:** Residue stability at 28-29% of the initial mass.
- o **DTA:** Return to a flat baseline, indicating the completion of all significant reactions.

The residue is thermally stable after major decomposition.

TGA and DTA analyses are complementary and confirm that SnS nanoparticles are stable up to approximately 750 °C. The main decomposition occurs between 750 °C and 950 °C, is a major exothermic process, and leads to a stable residue representing about 28-29% of the initial sample mass. This behavior is characteristic of the decomposition or oxidation of SnS at high temperatures, likely with significant sulfur volatilization.

Conclusion

This chapter described the synthesis and characterization of pure and Fe, Cu and Fe-Cu co-doped SnS nanoparticles. Meanwhile, the hydrothermal synthesis was chosen because of its simplicity, energy-saving and the shape control of final product. Careful experimental procedures were adopted for the synthesis of the various compositions, such as the above rigorous cleaning step taken to ensure the purity of the samples, while visible color changes were observed after doping.

X-ray diffraction (XRD) characterization revealed that the orthorhombic phase of SnS with high crystallinity was grown for all the samples. The absence of impurity peaks revealed the purity of the nanoparticles, and analysis further indicated that iron, copper dopants did not change the primary composition of the SnS crystalline as such although there was slight increase in the grain size and variation of the lattice parameters, indicating the successful substitution of the ions Sn^{2+} in the lattice by the dopants.

FTIR spectra supported this analysis as they allowed us to detect chemical bonds. The fact that the Sn-S band appeared in them supported the fact that the target compound was obtained. Moisture-related and carbonaceous residue bands were also observed, although no major new bonds were introduced by the doping that is to be expected, due to the low-concentration inclusion without evidence of the formation of secondary phases that could be detected by this technique.

Finally, the combined thermal analysis (ATG and ATD) evidenced the thermal stability of SnS nanoparticles up to around 750 °C and thereafter a great exothermic thermal decomposition, expected to occur between 750 and 950 °C, while the stable residue at 950 °C suggests the full conversion of the material. To conclude, as described in this chapter, pure as well as doped SnS nanoparticles were successfully synthesized through hydrothermal method and thorough characterization led to the useful information about the structural, chemical, and the thermal properties of the as-synthesized material, providing the basis for their further technological exploitation.

Chapter III : application

1. Photocatalysis

1.1. Introduction

Recently, dye-contaminated colored waste water from many businesses has become a major global problem due to its ability to pollute water supplies. These colors are widely utilized in many different sectors, including as textiles, plastics, paper, paints, pharmaceuticals, cosmetics, food processing, and so on, even though they are harmful to the environment.(29) These businesses pollute waterways by releasing dye-tainted wastewater into the environment. It is urgent to clean waste water and detoxify toxins because of the alarming level of water pollution and its detrimental effects. In recent years, photocatalysis employing heterogeneous semiconductor catalysts has become more and more popular as a straightforward, inexpensive, and highly effective method of using light to transform hazardous organic pollutants into non-toxic end products. Easy recovery, reuse, and a decrease in the formation of secondary waste are some of the alluring aspects of photoreduction using heterogeneous catalysts. Because photocatalysis employs solar energy, which is inherently plentiful, free, and unlimited, it tackles both environmental and energy problems when it comes to dye degradation. Because tin monosulfide (SnS) has a bandgap that is appropriate for the visible spectrum, it may make a great photocatalyst. SnS exhibits a low recombination velocity and a high stimulated carrier quantum yield.

Along with these photocatalytic properties, SnS offers several other benefits, including reduced toxicity, cost-effectiveness, constituent element abundance, and more. Even though SnS satisfies most of the requirements for a commercial photocatalyst that is scalable.

The present study includes a detailed investigation of the successful photodegradation of Methylene Blue (MB) dye using SnS nanoparticles as the photocatalyst. MB was chosen as the model pollutant because it is the most widely used and consumed textile dye.(29)

1.2. Definition of photocatalysis and processus

1.2.1. Definition

The terms "photo" (from the word "photon") and "catalyst," which refers to a material that changes the pace of a reaction when it is present, are combined to form the phrase "photocatalyst." Consequently, substances that alter a chemical reaction's pace upon exposure to light are known as photocatalysts. We call this process photocatalysis. Reactions that use a semiconductor and light are referred to as photocatalysis. A photocatalyst is a substrate that both absorbs light and catalyzes chemical processes. In essence, all photocatalysts are semiconductors. A process known as photocatalysis occurs when a semiconducting substance is exposed to light, creating an electron-hole pair.(30)

1.2.2. Types of photocatalysis

Based on how the reactants' physical states look, photocatalytic reactions may be divided into two categories.

- Homogeneous photocatalysis: This type of photocatalysis occurs when the semiconductor and reactant are in the same phase, such as a gas, solid, or liquid.
- Heterogeneous photocatalysis: This type of photocatalysis is defined as photocatalytic processes in which the reactant and semiconductor are in distinct phases.(30)

1.2.3. principle of the heterogeneous photocatalysis

In heterogeneous photocatalysis, a semiconductor is photoexcited by light absorption and a reaction with an adsorbed molecule. It may be defined as the catalysis of a photochemical reaction involving an interface between a solid and either a gas or a liquid. There are five separate phases in the photocatalytic process:

1. Reactants from the fluid phase diffusely migrate toward the photocatalyst's surface, including through its porosity.
2. At least one reagent is adsorbed onto the catalyst's surface.
3. Reaction in the adsorbed phase, which is where the photocatalytic reaction occurs.
4. Product desorption.
5. Products diffusely migrate from the catalyst's surface into the fluid phase.(31)

The formation of electron (e^-) / hole (h^+) pairs and the transfer of an electron from the valence band to the conduction band occur when photons with energy equal to or greater than the band gap of a semiconductor catalyst (TiO_2 , ZnO , Fe_2O_3 , ZnS , CdS , etc.) are absorbed (Figure 27 and Eq II.1). The formation of an electronic hole (h^+) in the valence band comes next (Eq II.1). At the same time, spontaneous adsorption occurs when a fluid phase (gas or liquid) is present. Depending on the redox potential of each adsorbate, molecules (A) with an electron-acceptor character (Figure 27 and Eq II.2) may experience electron transfer, while molecules (D) with an electron-donor character (Figure 27 and Eq II.3) may experience positive photo-holes. Lastly, recombination between electrons and holes is still feasible. It is accompanied by an exotherm (Eq II.4) and can occur in the volume (Figure 27) or on the semiconductor's surface (Figure 27).

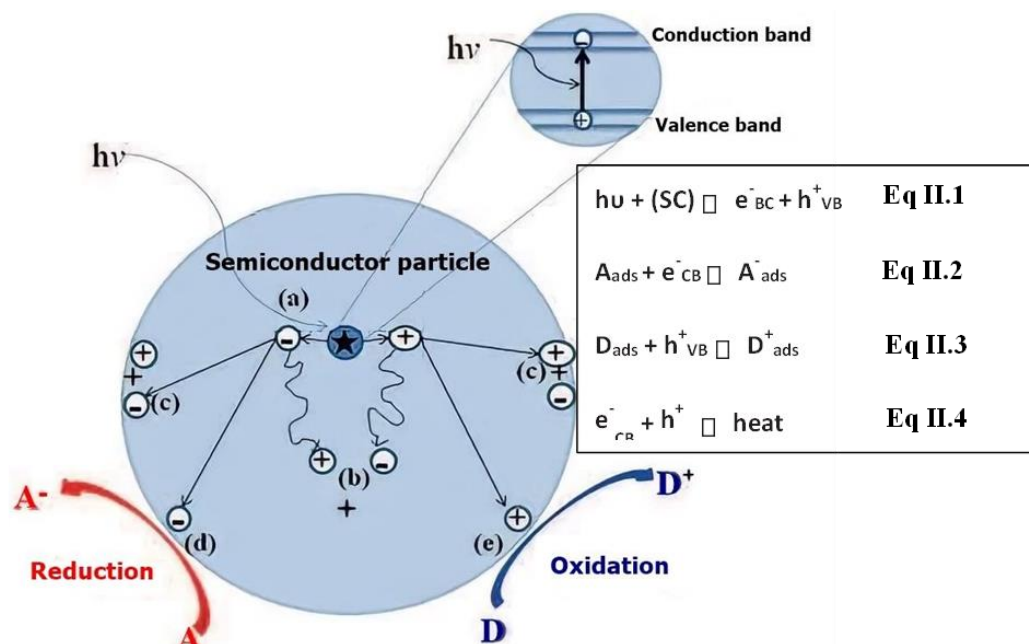
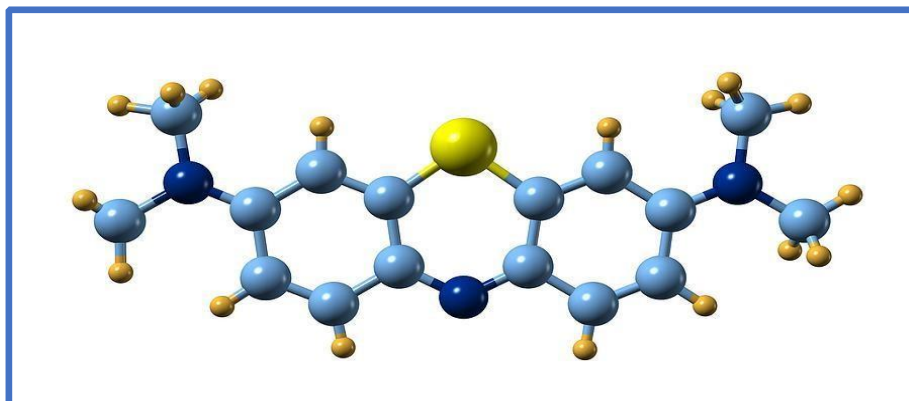


Figure 27 : General process of photocatalysis

1.3. Study of (MB) adsorption in the dark

The dye methylene blue is selected as a contaminant in this experiment. It belongs to the Quinoneimides group, which is a subgroup of Thiazines (sulfur dyes), where a closed ring made up of four carbon atoms, one nitrogen atom, and one sulfur atom joins two benzene rings. It is present in effluents that clearly harm the environment, and because of its toxicity, several research have been published on the potential removal of methylene blue by various adsorbents.



Item Name: Methylene blue (MB)

Molecular formula: $C_{16}H_{18}N_3SCl$

Density: 1.0g/mL at 20 °C

Wavelength (nm): The maximum absorption of light is near 670 nm

Molecular weight: 319.86 g/mol

Solubility :43,6 g/L in water at 25°C

Figure 28 : characteristic of BM and its molecular structure

1.3.1. Preparation of methylene blue solution

The methylene blue dye solution was prepared with a concentration of 10^{-5} mol/L. Using a spatula and an electronic balance, a quantity of 3.19 mg of the dye was weighed, then dissolved in an appropriate amount of distilled water (1 liter) and placed under magnetic agitation for about 15 minutes.



Figure 29: protocol of the study in the dark

1.3.2. Operating conditions and progress of the experiment

For each adsorption experiment performed, 0.8mg of the powder is mixed with 10mL of methylene blue solution. After that, the mixture was put on agitation in the dark for a different amount of time ranging from 10 to 60 min.

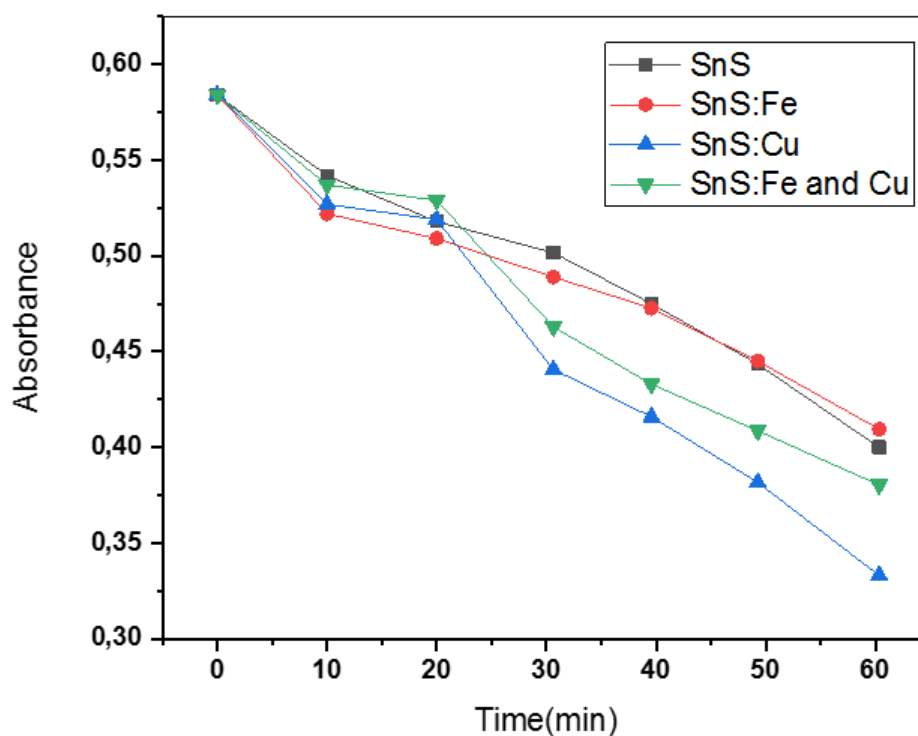


Figure 30 : Evolution of the absorbance spectrum of methylene blue

The results show a decrease in methylene blue (MB) absorbance over time in the dark, in the presence of pure and doped SnS nanoparticles. The experiment was designed to measure adsorption of nanoparticles to the dye in the absence of light (photocatalysis). Here are the results and evaluation:

For all the types of nanoparticles (pure SnS, SnS:Fe, SnS:Cu, SnS:Fe, and Cu), the absorbance of methylene blue decreased over time (60 min.) in darkness. The decrease in darkness was due to the phenomenon of adsorption. SnS nanoparticles adsorb the methylene blue molecules in the solution via their surface area. All SnS nanoparticles (pure and doped) adsorb MB in the dark. Copper doping (SnS:Cu) significantly increases this adsorption capacity, which will play an important role in photocatalytic applications since effective adsorption of the dye on the catalyst surface is often required for good photo-induced degradation.

Pure SnS (black) and SnS:Fe (red): These two samples exhibited a similar reduction in absorbance that was still significantly less than other snapshots. After 60 minutes, absorbance was about 0.40 pure SnS and 0.41 SnS:Fe. This means adsorption capacity was similar and that the added 1% Fe did not significantly improve dark adsorption. SnS:Fe and Cu (green): This sample had better adsorption than pure and SnS:Fe. At 60 minutes, its absorbance was about 0.38, which is lower than the previous 2. SnS:Cu (blue): This sample had the best dark adsorption performance. Its absorbance was approximately 0.33 at 60 minutes, which was the largest decrease of all the samples. All SnS nanoparticles (pure and doped) permanently demonstrate the ability to adsorb methylene blue in the dark. The attachment of copper (SnS:Cu), significantly improved this adsorption capacity, and is a very important factor for photocatalytic applications, since effective adsorption of the dye on the catalyst surface is often necessary for good degradation (photo-induced), if multiple mechanism/s.

Copper (Cu) doping appears to enhance the overall adsorption capacity of both SnS nanoparticle systems for methylene blue dye. This can arise from several factors: Increase in specific surface area: Doping can affect the size (X-ray diffractometry indicates SnS:Cu has a grain size of 24.16 nm compared to 22.12 nm in pure SnS), morphology, or porosity of the nanoparticles, effectively increasing the number of available sites for adsorption. Change in surface properties: Doping copper could affect the surface charge of the nanoparticle, or add new sites on the nanoparticle for a stronger interaction with methylene blue molecules. All SnS nanoparticle systems (pure and doped) are effective at adsorbing methylene blue in the dark. However, Cu doping (SnS:Cu) has improved the overall adsorption capacity for methylene blue. This is an ideal step if applying these photocatalytic materials, as very efficient decortration of dyes occurs in the photocatalytic material when adequate adsorption occurs of the dye onto the catalyst surface.

Copper has a stronger chemical affinity with methylene blue molecules, which could therefore enhance the binding of methylene blue to the surface of the nanoparticles. Iron doping alone does not appear to have a noticeable change in adsorption in the dark compared to pure SnS, wherein Fe-Cu co-doping shows only an improvement to adsorption capacity compared to pure SnS and SnS:Fe but not to the same degree exhibited with Cu alone.

- All SnS nanoparticles (both pure and doped) show the potential to adsorb methylene blue in the dark. when copper is added (SnS:Cu), the potential for adsorption is greatly enhanced. This is an important factor when considering photocatalytic applications, since efficient adsorption of a dye will often be a pre-requisite in order for photo-induced dye degradation to occur.

1.4. Photocatalytic tests

The visible light source for the photocatalysis experiment was a high-energy bulb. We added 20 mg of the catalyst powder to each of the four 50 ml BM solutions that we had produced. The samples were magnetically agitated in the dark for a maximum of 15 minutes before to exposure to visible light in order to create the adsorption-desorption equilibrium between the catalyst surfaces and the BM. About 5 milliliters of the aqueous solution are sampled every 15 minutes after exposure to visible light in order to quantify the absorbance (A%). Following each time period, the absorbance (A%) of the BM aqueous solution at 660 nm was measured using a UV-Vis spectrophotometer. The following formula is used to determine photocatalytic degradation:

$$\text{degradation (\%)} = \left(1 - \frac{C_t}{C_0}\right) \times 100$$

Where C_0 is the initial concentration of BM and C_t its concentrations measured over time.



Figure 31 : photocatalysis experiment

The result of the study are showing in figure 33 :

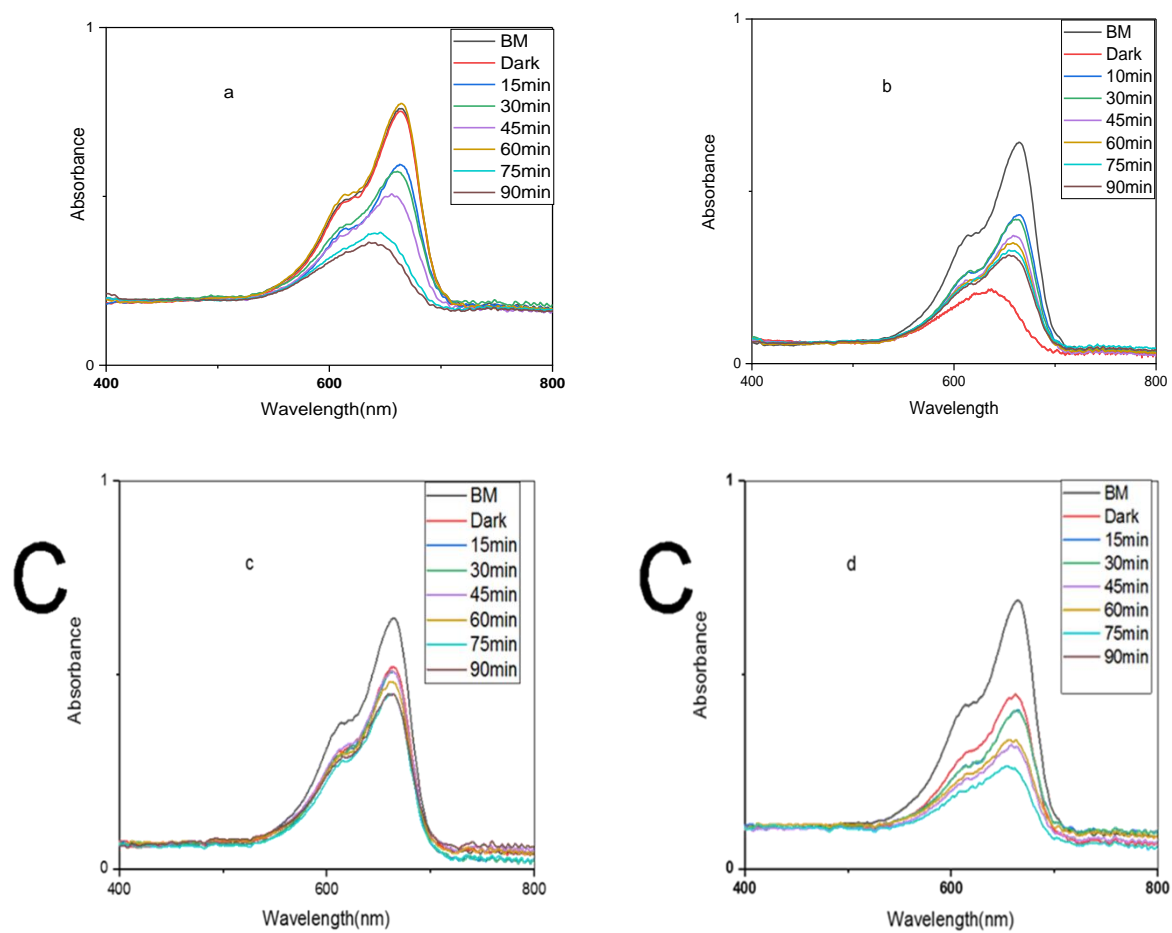


Figure 32: Evolution of the concentration of methylene blue over time and in the presence of SnS samples.

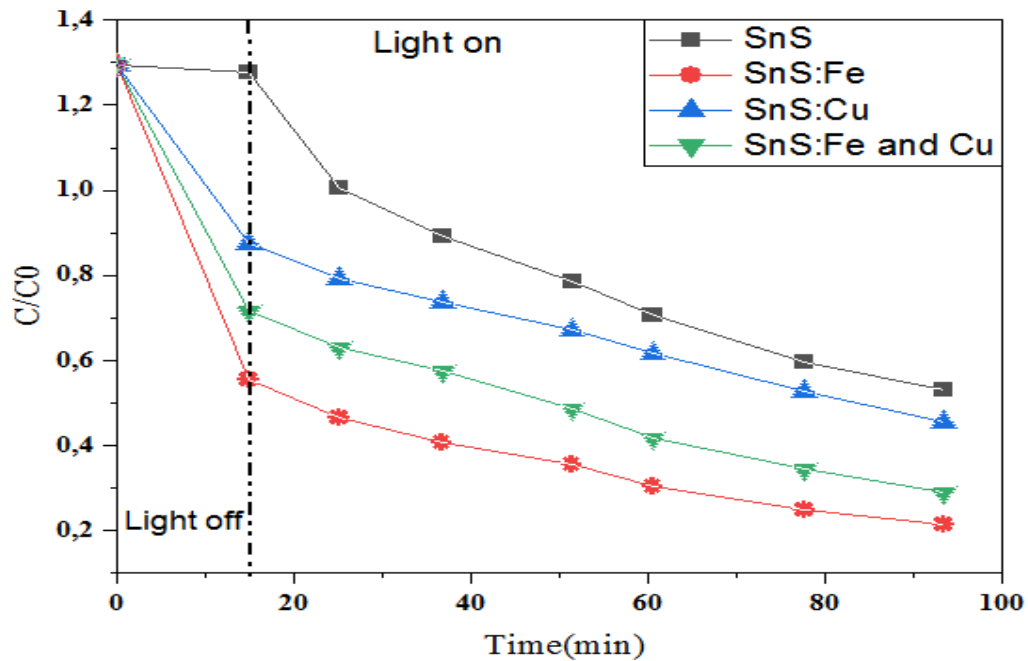


Figure 33: Degradation of BM

The graph displays the change in the relative concentration of methylene blue (C/C_0) over time in two different scenarios: "Light off," which is complete darkness, and "Light on," which is full light irradiation. The ability of SnS nanoparticles to break down the dye when exposed to light is assessed in this experiment. The comprehensive understanding is as follows:

- Phase of darkness ("Light off"):** For all samples (pure SnS, SnS:Fe, SnS:Cu, SnS:Fe, and Cu), the methylene blue concentration (C/C_0) falls during the first 15 minutes. The phenomenon of adsorption is the cause of this decline. Without the aid of light, methylene blue molecules adhere to the surface of SnS nanoparticles. Given that effective interaction between the catalyst and the pollutant is frequently required, the occurrence of this adsorption is a crucial sign for photocatalysis.

Phase of light irradiation ("Light on," starting at 15 minutes): The light is switched on at the fifteenth minute, and all samples' methylene blue concentrations continue to drop, albeit at varying speeds. The photocatalytic activity of the nanoparticles is indicated by this decrease when exposed to light. Comparison of the various samples' photocatalytic activity: The sample with the least amount of photocatalytic degradation is pure SnS (black squares). The curve's slope is the lowest, suggesting moderate degradation even while the concentration is decreasing. The relative concentration is remained at 0.53 at the conclusion of the experiment, which lasted for around 95 minutes under light.

SnS:Cu (Blue triangles): When compared to pure SnS, the copper-doped sample exhibits better photocatalytic activity. The final concentration is lower (around 0.45 after 95 minutes), and the curve drops more quickly. The greater adsorption capacity seen for this sample in the dark, which makes it easier for dye molecules to reach the catalyst surface, is most likely the cause of this enhanced performance.

SnS:Fe (red circles): When compared to pure SnS and SnS:Cu, iron doping significantly increases photocatalytic activity. After 95 minutes, the deterioration curve is noticeably more noticeable and reaches a relative concentration of roughly 0.22. This implies that iron is essential for increasing the photocatalytic process's quantum efficiency (for example, by enhancing the separation of photogenerated charges).

SnS:Fe and Cu (Green triangles) : In this experiment, the material co-doped with copper and iron exhibits the best overall photocatalytic performance. It has the sharpest deterioration curve and the lowest relative concentration (around 0.28 after 95 minutes). The co-doped sample's initial degradation rate is highly promising, despite SnS:Fe alone appearing slightly lower at the end.

Doping's effect on photocatalysis

The findings unequivocally show that doping, especially with iron (Fe) and co-doping (Fe and Cu), greatly increases the photocatalytic efficacy of SnS nanoparticles for methylene blue degradation. As dopants, iron and copper can produce intermediate energy levels or serve as sites for photogenerated charge carriers (holes and electrons) to recombine. To increase their availability to take part in degrading processes with the dye and reactive oxygen species, they should ideally trap charge carriers, blocking their quick recombination and extending their lifetime.

Iron and co-doping have a bigger impact on the material's electrical characteristics for increased photocatalytic efficiency, but copper's effect is most likely more connected to enhanced adsorption.

- SnS nanoparticles are active photocatalysts for the breakdown of methylene blue, as seen by the photocatalysis graph. Doping with copper enhances adsorption and, as a result, deterioration. On the other hand, photocatalytic efficiency is significantly impacted by iron doping and iron-copper co-doping most likely via improving charge separation and boosting the generation of reactive species, which are essential for the breakdown of pollutants. The potential of doped SnS nanoparticles for water treatment applications is demonstrated by these findings.

2. Photoluminescence

2.1. Introduction

A strong and non-destructive method for examining a material's optical and electrical characteristics, photoluminescence (PL) may provide details about its band structure, defect states, and recombination process

Luminescent semiconductor nano-crystals, especially II–VI semiconductors, have attracted great deal of attention in the past few decades due to their unique properties and potential. This II– VI compound semiconductor material has been studied for a variety of applications, such as optical coating, electro-optic modulator, photoconductors, field effect transistors, optical sensors, phosphors, and other light emitting materials.

Due to its favorable characteristics, such as earth abundance, low toxicity, and an appropriate direct bandgap tin (II) sulfide (SnS) has gained a lot of attention recently for use in a variety of optoelectronic applications, such as solar cells, photodetectors, and sensors.

SnS has historically had weak photoluminescence and a relatively low quantum efficiency, despite its potential. Ongoing studies, however, have uncovered intriguing facets of its PL behavior, especially in strongly doped systems and nanostructured forms. Research has demonstrated that by adjusting variables such synthesis settings, doping concentrations, and surface modifications, the photoluminescence of SnS may be greatly increased and regulated. Optimizing SnS-based devices requires an understanding of the complex interplay between the material's optical emission, defect chemistry, and structural properties.

The optical characteristics of ZnS NPs that we have attempted to alter and enhance via the use of various doping will be covered in depth in this chapter.

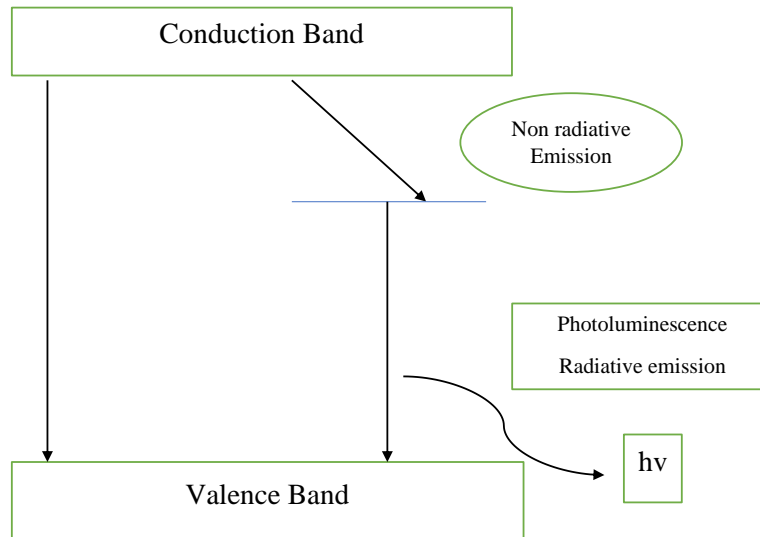


Figure 32 : Principle of photoluminescence

2.2 Property of each dopant

2.1.1. The Fe^{2+} Ion

Iron is a chemical element with the symbol Fe and atomic number 26. It is a **transition metal** in the 8th group of the periodic table, with a valence electron configuration of $[\text{Ar}] 3d^6 4s^2$. Iron exhibits a rich chemistry and has multiple possible oxidation states, with **+2 and +3 being the most common**, though others like +4 and +6 are also known. The choice of Fe^{2+} as a dopant is often strategic because its **ionic radius** (e.g., 0.77 Å for 4-coordinate tetrahedral, 0.75 Å for 6-coordinate high spin) can be close to that of certain host cations (like Zn^{2+} at ~0.74 Å for 4-coordinate or ~0.88 Å for 6-coordinate, or Sn^{2+} at ~1.12 Å for 4-coordinate) allowing for facile **substitutional doping** within the host lattice. This allows it to participate in various defect engineering and property modifications within materials.

2.1.2. The Cu^{2+} Ion

Copper is a chemical element with the symbol Cu and atomic number 29. It is a **transition metal** in the 11th group of the periodic table, with a valence electron configuration of $[\text{Ar}] 3d^{10} 4s^1$. Copper typically exhibits **+1 and +2 oxidation states**, with +2 being very common and stable, though +3 complexes are also known. The choice of Cu^{2+} as a dopant is particularly appealing because its

ionic radius (e.g., 0.71 Å for 4-coordinate tetrahedral or square planar, 0.87 Å for 6-coordinate octahedral) is often comparable to that of other divalent host cations (like Zn^{2+} at ~ 0.74 Å for 4-coordinate or ~ 0.88 Å for 6-coordinate, or Sn^{2+} at ~ 1.12 Å for 4-coordinate). This size compatibility facilitates its **incorporation as a substitutional impurity**, making it highly effective for manipulating the optical, electrical, and structural properties of materials for diverse applications.

2.2. Excitation spectrum

2.2.1. SnS doped Fe Cu NPs

The intensity of luminescence a sample emits as a function of the excitation light's wavelength is measured by excitation photoluminescence (PLE) spectra. The wavelengths at which a material absorbs light most effectively to produce luminescence are indicated as peaks in a PLE spectrum. We may infer the following information from the given PLE graph, which displays four spectra: pure SnS, SnS:1%Fe, SnS:1%Cu, and SnS:1%Fe 1%Cu.

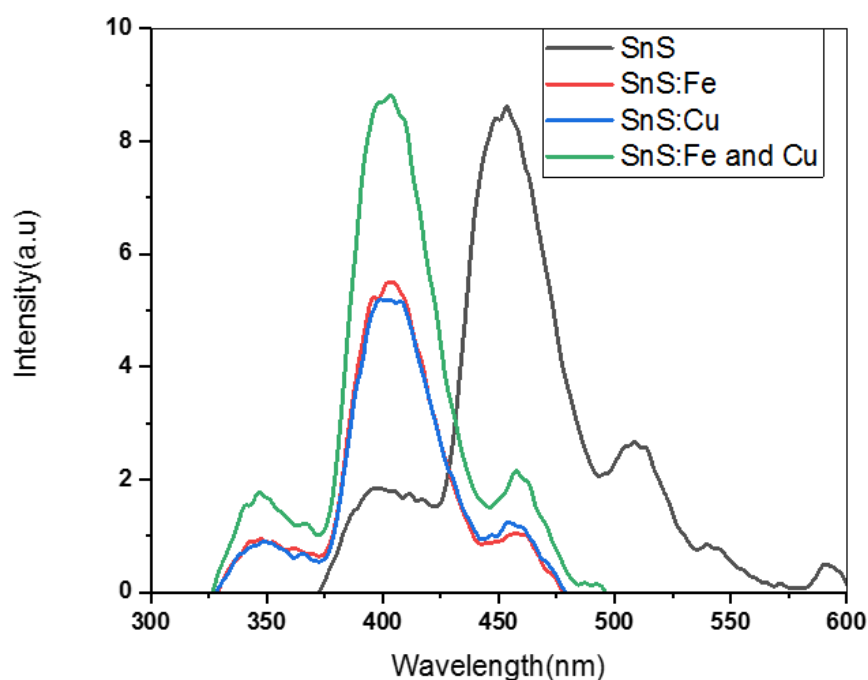


Figure 33: Excitement spectrum of SnS and doped SnS NPs

Pure SnS excitation peak (black curve): Around 450–460 nm, the primary excitation peak of pure SnS is broad and powerful. Around 500–520 nm, a secondary peak or weaker shoulder is also discernible. The intensity reaches a high peak of 8.5-9 arbitrary units (a.u.).

Doping's effect on peak position (shifting blue): The primary excitation peak for all doped materials (SnS:Fe, SnS:Cu, SnS:Fe, and Cu) changes considerably toward shorter wavelengths, about 400–405 nm. This blue shift shows that the addition of Fe and/or Cu alters the nanoparticles' optical absorption characteristics, increasing their ability to be excited by higher energy light (blue/violet). This could be the result of the dopants introducing new energy levels or altering the band gap.

Doping's impact on peak intensity : The red and blue curves are SnS:Fe and SnS:Cu, respectively: Their respective excitation peaks at 400-405 nm have significantly lower maximum intensities (about 5-5.5 u.a.) than the primary peak of pure SnS (at 450 nm), despite the fact that they both show a blue shift. This may indicate that at the new ideal excitation wavelength, single doping lowers the total efficiency of luminescence generation. Cu and SnS:Fe (green curve): At a peak of about 400–405 nm, this co-doped sample exhibits the highest excitation intensity of any sample, approaching 9 u.a. This suggests that co-doping with Fe and Cu greatly increases the light absorption efficiency, resulting in blue/violet luminescence that even outperforms pure SnS at its ideal excitation wavelength.

repercussions of the PLE findings : For situations where the excitation source is UV or blue light, the blue shift of the ideal excitation wavelengths is important. The co-doped sample (SnS:Fe and Cu) exhibits a rise in excitation intensity, indicating that it is best suited for light absorption and luminescence generation when excited at around 400 nm. Since effective light absorption is a requirement for effective photocatalysis, this discovery is in good agreement with the enhanced photocatalytic activity that was previously noted for this sample. Improved quantum efficiency for luminescence and catalytic activity can result from dopants' ability to produce new energy states that promote more effective electron-hole pair production or charge transfer.

2.3 Emission spectrum

2.3.1 SnS doped Fe Cu NPs

When a sample is excited by light of a particular wavelength, photoluminescence (PL) spectra show the intensity of light emitted by the sample as a function of wavelength. It is crucial to remember that 450 nm is the excitation wavelength used for these emission spectra. The ideal excitation seen in the PLE spectra for the un-doped samples. We can infer the following information from the given PL graph, which displays four spectra: pure SnS, SnS:1%Fe, SnS:1%Cu, and SnS:1%Fe 1%Cu.

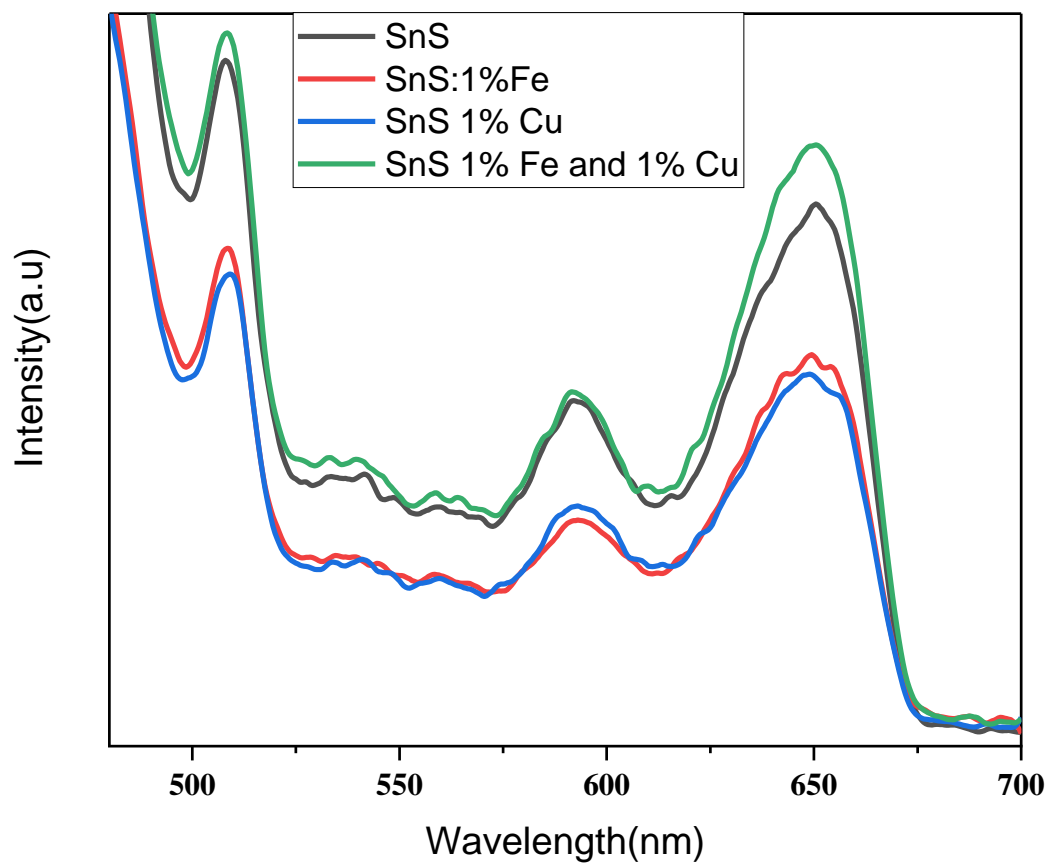


Figure 34 : Emission Spectrum of SnS and Fe Cu doped SnS NPs

Even with excitation at 450 nm, doping does not appear to significantly change the visual position of the main emission peaks. With significantly change in intensities, the primary bands mostly stay at the same wavelengths as for pure SnS (500 nm, 580-590 nm, 640-650 nm). This implies that rather than the basic energy levels of the SnS emission transitions, the dopants mainly influence non-radiative recombination processes.

Pure SnS emission spectrum (black curve): When excited at 450 nm, pure SnS shows a broad emission spectrum with multiple peaks or shoulders. A more intense peak appears around 640-650 nm (in the red region), while the main ones appear centered around 500 nm (in the green-blue region), and another around 580-590 nm (in the yellow-orange region). The existence of several broad emission bands indicates that the luminescence of pure SnS is complicated and may be caused by surface states, band-to-band recombination, or transitions involving defects (such as tin interstitials or sulfur vacancies). Either intrinsic or extrinsic defects functioning as radiative recombination centers may be responsible for the strongest peak at 640–650 nm. For pure SnS,

SnS:1%Cu (blue curve) and SnS:1%Fe (red curve): When all these doped samples are excited at 450 nm, the spectra reveal a notable decrease in photoluminescence intensity in comparison to pure SnS. The curves are flatter, and the peaks—especially the one at 640–650 nm—are substantially less intense. This suggests that 1% Fe or Cu doping functions as a non-radiative recombination center. Stated differently, the photoluminescence efficiency is decreased because the charge carriers (electrons and holes) produced by excitation at 450 nm tend to recombine via non-light-producing pathways. Electrons and holes are "trapped" by these dopant-induced defects, which stop them from radiatively recombining.

SnS: 1%Cu and 1%Fe (green curve): The emission intensity of the co-doped sample is marginally higher than that of the individually doped samples (especially around 640-650 nm), This implies that the luminescence quenching effect seen with single doping can be somewhat mitigated by co-doping. After doping with Fe and Cu, a very significant outcome that is frequently desired for photocatalytic applications is the quenching, or reduction, in photoluminescence intensity. Even when excited at the ideal wavelength, low photoluminescence emission signifies less electron-hole recombination at the semiconductor surface. The charge carriers are more available to take part in chemical reactions, such as producing reactive oxygen species for the degradation of pollutants, if they do not recombine radiatively, or by emitting light. Combining these findings with those of photocatalysis reveals that the doped samples, which have lower PL, have higher photocatalytic activity. This lends credence to the theory that Fe and Cu serve as effective charge carrier traps, encouraging their separation and surface transfer to start the methylene blue degradation process.

Conclusion

This chapter concentrated on assessing the application properties of both pure and doped SnS nanoparticles, particularly their photoluminescent qualities and potential as photocatalysts for the degradation of methylene blue.

We began the photocatalysis section by emphasizing the importance of treating dye-contaminated wastewater and the potential of heterogeneous photocatalysis. All SnS nanoparticles have the ability to adsorb methylene blue, according to the dark adsorption study. In particular, it was highlighted that copper doping (SnS:Cu) significantly increases this capacity, highlighting the significance of effective initial adsorption for degradation processes. The beneficial effect of doping on degradation efficiency was amply demonstrated by photocatalytic tests conducted in visible light. The photodegradation of methylene blue is significantly enhanced by iron doping and iron-copper co-doping (SnS:1%Fe 1%Cu), whereas pure SnS exhibits limited activity. This improvement is explained by the dopants' capacity to trap charge carriers (holes and electrons), encouraging their separation and lowering their recombination, which increases the amount of reactive species available for pollutant degradation.

The optical property analysis was supplemented by the photoluminescence (PL) section. Excitation spectra (PLE) demonstrated that iron and copper doping causes a blue-shift in the SnS nanoparticles' ideal excitation wavelengths, increasing their excitability by blue/violet light. The Fe-Cu co-doped sample was notable for having the highest excitation intensity, which suggests improved light absorption that results in luminescence. On the other hand, all doped nanoparticles showed notable photoluminescence quenching when compared to pure SnS in the emission spectra (PL), which were recorded with excitation at 400 nm (the optimal PLE peak of the doped samples). One important sign of decreased electron-hole recombination through radiative pathways is this decrease in light emission.

To sum up, this chapter's findings demonstrate a clear relationship between SnS nanoparticles' optical characteristics and photocatalytic activity. In addition to increasing light absorption capacity (PLE), doping with iron and copper, especially Fe-Cu co-doping, is important because it decreases recombination processes, which increases the availability of charge carriers for degradation reactions (PL quenching). This results in a higher rate of methylene blue degradation when exposed to visible light. These results support the doped SnS nanoparticles' encouraging potential for environmental uses, especially photocatalytic wastewater treatment.

General conclusion

In this study, both pure and iron (Fe^{2+}) or copper (Cu^{2+}) doped tin sulfide (SnS) nanoparticles were synthesized and characterized in detail. Their possible uses, mainly in photocatalysis, were also assessed. The versatility and importance of SnS nanostructures have been emphasized by this work, which falls within the quickly growing field of semiconductor nanomaterials. Reviewing nanoscience and nanotechnology, laying out the theoretical underpinnings and various uses of nanoparticles, and defending the selection of SnS as a promising material for optoelectronic devices and environmental applications were the first steps in the work.

It has been confirmed that hydrothermal synthesis is a successful method for producing doped and pure SnS nanoparticles with good crystallinity. While observing an impact on grain size, X-ray diffraction (XRD) analyses verified the formation of the orthorhombic phase of SnS and showed that Fe and Cu dopants were successfully incorporated into the lattice without forming secondary phases. The presence of residues and the creation of Sn-S bonds were both confirmed by FTIR spectroscopy. Thermogravimetric (TGA) and Differential Thermal (DTA) analyses demonstrated that SnS nanoparticles were thermally stable up to high temperatures, after which they underwent a significant exothermic breakdown. Results from application investigations were very positive. All SnS nanoparticles showed adsorption capacity for methylene blue in the dark, with copper doping greatly enhancing this capacity. Doping, especially with iron and co-doping, significantly boosts the efficiency of methylene blue degradation under visible light, according to photocatalytic tests. The materials' optical qualities are directly related to this improvement. (PLE) spectra showed that the doped samples, particularly the co-doped sample, had a blue shift and a higher light absorption efficiency. Importantly, the doped nanoparticles' emission (PL) spectra revealed photoluminescence quenching. This decrease in light emission is proof that there is less charge carrier recombination, which increases the number of electrons and holes available for redox reactions at the catalyst surface, which is what propels photocatalytic activity. Incorporating iron and copper into SnS nanoparticles can optimize their optical and electronic properties, as this work has successfully synthesized and characterized both pure and doped SnS nanoparticles. As a result, they perform significantly better as photocatalysts for the breakdown of organic pollutants. These findings present encouraging opportunities for the application of doped SnS nanoparticles in novel wastewater treatment and other environmental applications.

Bibliographic references

1. Bayda S, Adeel M, Tuccinardi T, Cordani M, Rizzolio F. The History of Nanoscience and Nanotechnology: From Chemical–Physical Applications to Nanomedicine. *Molecules*. 27 déc 2019;25(1):112.
2. A. D. Pomogailo, and V. N. Kestelman. “Nanoparticles in Materials Chemistry and in the Natural Sciences (Introduction.
3. Ramsden JJ. What is Nanotechnology? In: *Applied Nanotechnology* [Internet]. Elsevier; 2018 [cité 17 mars 2025]. p. 3-13. Disponible sur: <https://linkinghub.elsevier.com/retrieve/pii/B9780128133439000020>
4. Zahir Asmaa_Matser Thesis_2022-2023.
5. Messalti AS. Investigations des propriétés photoluminescentes des nanoparticules de ZnS dopées. [Doctorat]. [Sétif]: Farhat Abbas; 2021.
6. Sajid M, Plotka-Wasyłka J. Nanoparticles: Synthesis, characteristics, and applications in analytical and other sciences. *Microchem J*. mai 2020;154:104623.
7. Anu Mary Ealia S, Saravanakumar MP. A review on the classification, characterisation, synthesis of nanoparticles and their application. *IOP Conf Ser Mater Sci Eng*. nov 2017;263:032019.
8. Kumari S, Raturi S, Kulshrestha S, Chauhan K, Dhingra S, András K, et al. A comprehensive review on various techniques used for synthesizing nanoparticles. *J Mater Res Technol*. nov 2023;27:1739-63.
9. Rawat RS. Dense Plasma Focus - From Alternative Fusion Source to Versatile High Energy Density Plasma Source for Plasma Nanotechnology. *J Phys Conf Ser*. 24 mars 2015;591:012021.
10. Terna AD, Elemike EE, Mbonu JI, Osafire OE, Ezeani RO. The future of semiconductor nanoparticles: Synthesis, properties and applications. *Mater Sci Eng B*. oct 2021;272:115363.
11. Minhaz Abedin. A SELF-ADJUSTING LIN-LOG ACTIVE PIXEL FOR WIDE DYNAMIC RANGE CMOS IMAGE SENSOR [Internet]. Unpublished; 2015 [cité 18 mars 2025]. Disponible sur: <http://rgdoi.net/10.13140/RG.2.1.3871.8965>
12. Divsar F. Introductory Chapter: Quantum Dots. In: Divsar F, éditeur. *Quantum Dots - Fundamental and Applications* [Internet]. IntechOpen; 2020 [cité 24 mars 2025]. Disponible sur: <https://www.intechopen.com/books/quantum-dots-fundamental-and-applications/introductory-chapter-quantum-dots>
13. Divsar F, éditeur. *Quantum Dots - Fundamental and Applications* [Internet]. IntechOpen; 2020 [cité 22 mars 2025]. Disponible sur: <https://www.intechopen.com/books/quantum-dots-fundamental-and-applications>

14. Setout, Refsa N Malika. Synthèse et caractérisation des couches minces de Sulfure d'étain dopées : Application au Traitement des eaux. [MASTER]. 'Ain Témouchent – Belhadj Bouchaib; 2023.
15. Sohila S, Rajalakshmi M, Ghosh C, Arora AK, Muthamizhchelvan C. Optical and Raman scattering studies on SnS nanoparticles. J Alloys Compd. mai 2011;509(19):5843-7.
16. DEKHILI M. Effet du substrat sur les propriétés structurales optiques et électriques des couches minces de sulfure d'étain (SnS) [MASTER]. MOHAMMED SEDDIK BEN YAHIA - JIJEL; 2022.
17. Tritsarlis GA, Malone BD, Kaxiras E. Optoelectronic properties of single-layer, double-layer, and bulk tin sulfide: A theoretical study. J Appl Phys. 21 juin 2013;113(23):233507.
18. Sana, Nougali B Malika. ETUDE MICROSTRUCTURALE ET OPTIQUE DES COUCHES MINCES DU DISULFURE D'ETAIN (SnS₂) DEPOSEES PAR SPRAY PYROLYSE ULTRASONIQUE [MASTER]. Ibn Khaldoun - Tiaret; 2016.
19. Hegde SS, Kunjomana AG, Chandrasekharan KA, Ramesh K, Prashantha M. Optical and electrical properties of SnS semiconductor crystals grown by physical vapor deposition technique. Phys B Condens Matter. mars 2011;406(5):1143-8.
20. Banai RE, Burton LA, Choi SG, Hofherr F, Sorgenfrei T, Walsh A, et al. Ellipsometric characterization and density-functional theory analysis of anisotropic optical properties of single-crystal α -SnS. J Appl Phys. 7 juill 2014;116(1):013511.
21. Koteeswara Reddy N, Devika M, Gopal ESR. Review on Tin (II) Sulfide (SnS) Material: Synthesis, Properties, and Applications. Crit Rev Solid State Mater Sci. 2 nov 2015;40(6):359-98.
22. Norton KJ, Alam F, Lewis DJ. A Review of the Synthesis, Properties, and Applications of Bulk and Two-Dimensional Tin (II) Sulfide (SnS). Appl Sci. 26 févr 2021;11(5):2062.
23. Kumar P, Kumar R. Synthesis process of functionalized ZnO nanostructure for additive manufacturing: a state-of-the-art review. In: Additive Manufacturing with Functionalized Nanomaterials [Internet]. Elsevier; 2021 [cité 18 avr 2025]. p. 135-53. Disponible sur: <https://linkinghub.elsevier.com/retrieve/pii/B9780128231524000028>
24. Byrappa K, Yoshimura M. Handbook of hydrothermal technology: a technology for crystal growth and materials processing. Norwich, N.Y: Noyes Publications; 2001.
25. Jayatissa YXGAH, Yu Z, Chen X, Li M. Hydrothermal Synthesis of Nanomaterials. J Nanomater [Internet]. mars 2020 [cité 19 avr 2025];2019. Disponible sur: <https://link.gale.com/apps/doc/A622149891/AONE?u=anon~bcffc934&sid=googleScholar&xid=3dae4361>
26. Yen WM, Yamamoto H, Yen WM /Shionoya Shigeo(deceased). Fundamentals of Phosphors. 1^{re} éd. 2018.

27. Arun KJ, Kumar KS, Batra AK, Aggarwal MD, Francis PJJ. Surfactant Free Hydrothermal Synthesis of CdO Nanostructure and Its Characterization. *Adv Sci Eng Med*. 1 sept 2015;7(9):771-5.
28. Djellabi riadh. contribution de la photocatalyse à l'élimination des polluants industriels [Thèse de doctorat]. [ANNABA]: BADJI MOKHTAR - ANNABA; 2014.
29. N A, Philip RS, Mathew M. Photocatalytic activities of SnS thin films deposited at room temperature. *Appl Surf Sci Adv*. févr 2023;13:100374.
30. Ameta R, Solanki MS, Benjamin S, Ameta SC. Photocatalysis. In: *Advanced Oxidation Processes for Waste Water Treatment* [Internet]. Elsevier; 2018 [cité 8 juin 2025]. p. 135-75. Disponible sur: <https://linkinghub.elsevier.com/retrieve/pii/B9780128104996000061>
31. Boudjadi I. el synthesis of $\text{CaFe}_{1-x}\text{Cu}_x\text{O}_3$ perovskite for photocatalytic application. [Sétif]: Ferhat Abbas University; 2021.

Abstract

This study aims to synthesize and characterize pure and doped (Fe, Cu) tin sulfide (SnS) nanoparticles via the hydrothermal method. Analyses confirmed their crystalline structure and the successful incorporation of dopants. Key results show that doping, particularly with iron and Fe-Cu co-doping, significantly enhances methylene blue adsorption capacity and especially photocatalytic efficiency under visible light. This improvement is linked to enhanced light absorption and reduced charge carrier recombination, making these nanoparticles promising for wastewater treatment.

Keywords: tin sulfide, iron and cooper, hydrothermal method, nanoparticles, photocatalytic.

Résumé

Cette étude vise à synthétiser et caractériser des nanoparticules de sulfure d'étain (SnS), pures et dopées (Fe, Cu), via la méthode hydrothermale. Les analyses ont confirmé leur structure cristalline et l'incorporation réussie des dopants. Les résultats clés montrent que le dopage, particulièrement avec le fer et la co-dopage Fe-Cu, améliore significativement la capacité d'adsorption du bleu de méthylène et surtout l'efficacité photocatalytique sous lumière visible. Cette amélioration est liée à une meilleure absorption lumineuse et à une réduction de la recombinaison des porteurs de charge, rendant ces nanoparticules prometteuses pour le traitement des eaux usées.

Mots-clés : sulfure d'étain, fer et cuivre, méthode hydrothermale, nanoparticules, photocatalytique

ملخص

تَهْدَفُ هَذِهِ الدِّرَاسَةُ إِلَى تَرْكِيبِ وَتَحْلِيلِ جُسَيْمَاتٍ نَانَوِيَّةٍ مِنْ كَبْرَيْتِيدِ الْقَصْدِيرِ النَّقِيَّةِ وَالْمُطَعَّمَةِ (بِالْحَدِيدِ وَالنُّحَاسِ)، عَنْ طَرِيقِ الطَّرِيقَةِ الْهَيْدُرُوثيرْمَالِيَّةِ. أَكَّدَتِ النَّحَالِيلُ بُنْيَانَهَا الْبُلُورِيَّةَ وَإِدْمَاجَ الْمَوَادِّ الْمُضَافَةِ بِنَجَاحٍ. تُظْهِرُ النَّتَائِجُ الرَّئِيسِيَّةُ أَنَّ النَّطْعِيمَ، وَخَاصَّةً بِالْحَدِيدِ وَالطَّعْمِ الْمَزْدُوجِ لِلْحَدِيدِ وَالنُّحَاسِ، يُحَسِّنُ بِشَكْلٍ مُلْحُوظٍ قُدْرَةَ الْاِمْتِزَازِ لِلْأَزْرَقِ الْمِيثِيلِينِيِّ وَفَاعَلِيَّةَ التَّحْفِيزِ الضَّوئِيِّ تَحْتَ الضَّوءِ الْمَرْبِيِّ. يَرْتَبِطُ هَذَا التَّحْسِينُ بِزِيَادَةِ امْتِصَاصِ الضَّوءِ وَتَقْلِيلِ إِعَادَةِ اتِّحَادِ حَامِلِي الشُّحْنَةِ، مِمَّا يَجْعَلُ هَذِهِ الْجُسَيْمَاتِ النَّانَوِيَّةَ وَاعِدَةً لِمُعَالَجَةِ مِيَاهِ الصَّرْفِ الصَّحِيِّ

الكلمات المفتاحية: كبريتيد القصدير، الحديد والنحاس، الطريقة الهيدروحرارية، الجسيمات النانوية، التحفيز الضوئي